STEM CELLS

Developmental DNA demethylation is a determinant of neural stem cell identity and gliogenic competence

Ian C. MacArthur[1,2,3], Liyang Ma[1,2,3], Cheng-Yen Huang[1,2,3], Hrutvik Bhavsar[1,2,3], Masako Suzuki[4], Meelad M. Dawlaty[1,2,3]*

DNA methylation is extensively reconfigured during development, but the functional significance and cell type–specific dependencies of DNA demethylation in lineage specification remain poorly understood. Here, we demonstrate that developmental DNA demethylation, driven by ten-eleven translocation 1/2/3 (TET1/2/3) enzymes, is essential for establishment of neural stem cell (NSC) identity and gliogenic potential. We find that loss of all three TETs during NSC specification is dispensable for neural induction and neuronal differentiation but critical for astrocyte and oligodendrocyte formation, demonstrating a selective loss of glial competence. Mechanistically, TET-mediated demethylation was essential for commissioning neural-specific enhancers in proximity to master neurodevelopmental and glial transcription factor genes and for induction of these genes. Consistently, loss of all three TETs in embryonic NSCs in mice compromised glial gene expression and corticogenesis. Thus, TET-dependent developmental demethylation is an essential regulatory mechanism for neural enhancer commissioning during NSC specification and is a cell-intrinsic determinant of NSC identity and gliogenic potential.

INTRODUCTION

Methylation of the 5-position carbon of cytosine (5mC) in DNA is a critical epigenetic modality regulating gene expression during mammalian development (*1*). Its presence at gene regulatory elements canonically represses gene expression (*1*). DNA methylation is deposited by the de novo DNA methyltransferases DNMT3A/B and is maintained upon replication by the maintenance methyltransferase DNMT1 (*1*). DNA demethylation can occur passively by failure to maintain 5mC during replication or actively via oxidation by the ten-eleven translocation (TET) family of dioxygenases (TET1, TET2, and TET3) (*2*). TET enzymes oxidize 5mC to 5-hydroxymethylcytosine (5hmC), which can evade DNMT1 during cell division leading to passive demethylation or remain as a stable epigenetic mark where it is generally associated with gene activation (*2*–*4*). TET enzymes can further oxidize 5hmC to 5-formylcysotine and 5-carboxylcytosine, which are removed from the genome by thymine DNA glycosylase and the base excision repair pathway (*5*, *6*). Methylation at CpG dinucleotides is rapidly acquired in postimplantation mammalian embryos, rising from 20% genome-wide at embryonic day 3.5 (E3.5) to 80% by E6.5 in mouse, and is deposited in part to restrict cell fate and silence repetitive DNA (*1*). It has been proposed that this genomic hypermethylation in mammals and other vertebrates may have facilitated the use of DNA demethylation as a means of defining cis-regulatory elements during development (*7*, *8*). Despite the observation that enhancers become developmentally demethylated (*9*), the functional impact of loss of TET enzymes and the demethylation machinery on enhancer chromatin state and lineage specification remains poorly understood.

Coincident with the discovery that TET enzymes are DNA dioxygenases was the finding that 5hmC is highly enriched in the nervous system compared to other somatic tissues (*10*), leading to great interest in the role of TET enzymes in neurodevelopment and neural physiology (*11*). All three TET enzymes are expressed, and 5hmC is highly abundant in the embryonic brain (*12*, *13*), particularly in neural progenitor cells (*14*). Moreover, mutations in *TET* genes and alterations in 5mC and 5hmC have been identified in individuals with intellectual disability and other neurodevelopmental disorders (*11*). Despite this compelling evidence for a crucial neurodevelopmental role for TET enzymes and DNA demethylation, functional studies of complete TET loss in the developing nervous system are lacking. This is in part due to the high degree of redundancy between *Tet* paralogs and the early embryonic lethality of *Tet1/2/3* triple knockout (TKO) embryos at gastrulation. Global loss of TET1 or TET2, which is compatible with life, and loss of TET3, which leads to perinatal lethality, do not grossly compromise neurodevelopment (*15*–*18*). In contrast, TET TKO embryos arrest at late gastrulation (*19*). This has prevented a comprehensive understanding of the full scope of TET functions and DNA demethylation during neurodevelopment.

Recent single-cell multiomic analyses of *Tet* TKO chimeric embryos have provided some insights into the ability of TET-deficient embryonic stem cells (ESCs) to contribute to primitive neuroectodermal progenitors around the time of neural induction (*20*, *21*). However, the functional impact of loss of TET-mediated developmental demethylation in the neural lineage remains undefined. First, it is not known how TET-dependent demethylation regulates neural stem cell (NSC) specification and NSC differentiation into mature neural cell types, especially into cells arising at late embryonic time points. Second, the ability of developmental demethylation to shape chromatin state and the way this contributes to gene regulation and cell fate determination remain poorly defined. In this study, using an ESC-to-NSC differentiation platform, we have identified a critical requirement for TET-mediated DNA demethylation in establishment of NSC identity and gliogenic competence. *Tet* TKO NSCs expressed reduced levels of neural markers and had limited self-renewal. While they retained the ability to differentiate into neurons, albeit with reduced

[1]Ruth L. and David S. Gottesman Institute for Stem Cell and Regenerative Medicine Research, Albert Einstein College of Medicine, 1301 Morris Park Ave, Bronx, NY 1046142, USA. [2]Department of Genetics, Albert Einstein College of Medicine, 1301 Morris Park Ave, Bronx, NY 10461, USA. [3]Department of Developmental & Molecular Biology, Albert Einstein College of Medicine, 1300 Morris Park Ave, Bronx, NY 10461, USA. [4]Department of Nutrition, Texas A&M University, 2253 TAMU, Carter Mattil 214A, College Station, TX 77840, USA.
*Corresponding author. Email: meelad.dawlaty@einsteinmed.edu

efficiency, they could not differentiate into astrocytes and oligodendrocytes, indicating a severe and selective loss of glial competence. Master neurodevelopmental transcription factors (TFs), including those of the *Nfi* and *Olig* families of glial TFs, were severely downregulated in TKO NSCs. In the proximity of these TF genes, we identified hundreds of neural-specific enhancers whose developmental demethylation was TET dependent. Both the commissioning and activation of these enhancers were severely compromised in the absence of TET enzymes, underpinning the reduced expression of neural TFs and loss of glial competence. Consistent with our in vitro findings, conditional knockout of all three *Tet* genes in dorsal telencephalic NSCs compromised expression of glial genes and proper development of cortical structures. Our findings establish TET-mediated developmental demethylation of neural enhancers as a critical epigenetic modality required for the establishment of NSC identity and gliogenic competence.

RESULTS

NSCs specified in the absence of TET enzymes have compromised identity and self-renewal

To establish the function of TET enzymes and DNA demethylation during NSC specification, we generated *Tet1/2/3* TKO ESCs by deleting *Tet1/2/3* exon 4 (Fig. 1A), loss of which is known to result in formation of nonsense transcripts and complete loss of TET proteins (*22*). We confirmed deletion of *Tet1/2/3* exon 4 in TKO ESCs by polymerase chain reaction (PCR) (fig. S1A) and complete loss of *Tet1/2/3* exon 4–containing mRNA by reverse transcription quantitative PCR (RT-qPCR) (fig. S1B). Consistent with previous studies (*22*, *23*), *Tet* TKO ESCs maintained normal growth and morphology in culture (fig. S1C). Three wild-type (WT) and two TKO ESC clones were differentiated to NSCs following a well-established protocol that entails differentiation of ESCs to embryoid bodies (EBs) for 4 days, followed by culturing on adherent plates in defined growth medium for 9 days and lastly expanding NSCs in neural medium (Fig. 1B) (*24*, *25*). This is a standard method for producing NSCs capable of prolonged culture and multilineage differentiation (*24*). TKO ESCs efficiently formed EBs that were comparable in size and morphology to WT EBs during suspension and adherent phases of differentiation (fig. S1C). Both WT and TKO cultures yielded NSCs that appeared morphologically normal and grew comparably to WT during the first week [Fig. 1, C (left and middle) and D]. However, TKO NSCs could not be maintained in culture beyond 2 weeks (~4 passages), indicating a defect in self-renewal [Fig. 1, C (right) and D]. Both WT and TKO NSCs stained positive for NSC markers SRY-box transcription factor 1 (SOX1), SOX2, and NESTIN (Fig. 1E), confirming acquisition of an NSC state. However, the transcript levels of these and other core neurodevelopmental TFs *Pax6* and *Otx1* were robustly reduced in TKO NSCs (Fig. 1F), indicative of compromised NSC identity. These results suggest that, while loss of TET enzymes allows specification of NSCs from ESCs, the resulting NSCs have limited self-renewal and altered identity with aberrant expression of core neural TFs, which may affect their ability to form neural cell types.

Tet TKO NSCs have reduced neuronal differentiation potential and complete loss of glial competence

To assess the effects of TET loss on NSC multipotency, we differentiated WT and TKO NSCs (1 week after their specification and before loss of self-renewal) to neurons and glial cell types (astrocytes and oligodendrocytes) following defined protocols for each cell type. When differentiated to neurons, TKO NSCs were able to form $TUJ1^+$ neurons (Fig. 2A), but expression of *Tubb3*, *Dcx*, and *Rbfox3* mRNA was significantly reduced in TKO neuronal cultures (Fig. 2B). This indicates that TET loss reduces but does not categorically compromise neuronal differentiation. In notable contrast, when differentiated to astrocytes, TKO NSCs could not form glial fibrillary acidic protein–positive ($GFAP^+$) astrocytes (Fig. 2C), and expression of key astrocytic markers *Gfap*, *Aqp4*, and *S100b* was undetectable in these cultures (Fig. 2D), confirming a complete inability of TKO NSCs to differentiate into astrocytes. Likewise, when differentiated to oligodendrocytes, TKO NSCs failed to yield oligodendrocyte marker 4 ($O4)^+$ oligodendrocytes (Fig. 2E), and key oligodendrocyte markers *Myrf*, *Sox10*, and *Plp1* were not induced in these cultures (Fig. 2F), indicating a complete impairment in oligodendrocyte differentiation. Together, the selective inability of TKO NSCs to form astrocytes and oligodendrocytes reveals a general block in glial differentiation and supports a critical role for TET enzymes in establishing NSC gliogenic competence.

Loss of TET enzymes results in failure to establish neurodevelopmental gene expression programs, including activation of the *Nfi* and *Olig* families of glial TFs

To define the transcriptional effects of TET loss during NSC specification, we profiled transcriptomes of WT and TKO ESCs and NSCs by RNA sequencing (RNA-seq). Principal components analysis (PCA) revealed high correspondence between biological replicates for each cell type and genotype (fig. S2A). PC1, representing differences between ESC and NSC transcriptomes, indicated that WT and TKO NSCs clustered closely together and away from WT and TKO ESCs, highlighting that WT and TKO NSCs had undergone comparable transcriptional changes during differentiation. PC2, representing differences between WT and TKO cells, indicated that WT and TKO NSCs differed more greatly from each other than WT and TKO ESCs (fig. S2A), supporting a more robust role for TET enzymes in regulating gene expression upon ESC differentiation than in steady-state ESCs. Consistently, we identified 2324 differentially expressed genes (DEGs) (1080 up-regulated and 1244 down-regulated) between TKO and WT NSCs compared to 488 DEGs (234 up-regulated and 254 down-regulated) between TKO and WT ESCs (Fig. 3A). Only 142 of these DEGs were shared between the ESC and NSC states, which were excluded from NSC DEGs to obtain 2182 NSC-specific DEGs (1177 down-regulated and 1005 up-regulated) (Fig. 3B and fig. S2B). Gene ontology analysis revealed that NSC-specific down-regulated genes were enriched for neurodevelopmental processes including gliogenesis (Fig. 3C), consistent with the observed block in TKO NSC glial differentiation (Fig. 2, C to F). NSC-specific up-regulated genes were enriched primarily for mesodermal development terms (fig. S2C), in line with the well-described derepression of mesoderm genes that accompanies loss of TET enzymes (*26*). Of the 1177 NSC-specific down-regulated genes, the majority (841, 71%) were genes that were normally induced during WT ESC-to-NSC differentiation, while the rest (336, 29%) were genes that either remained unchanged or were down-regulated (Fig. 3D). Together, these results affirm a neurodevelopmental role for NSC-specific down-regulated genes and demonstrate a failure to properly induce them in the absence of TET enzymes.

The NSC-specific down-regulated genes included many neurodevelopmental TFs (Fig. 3E), including *Sox1*, *Pax6*, and *Otx1*, which

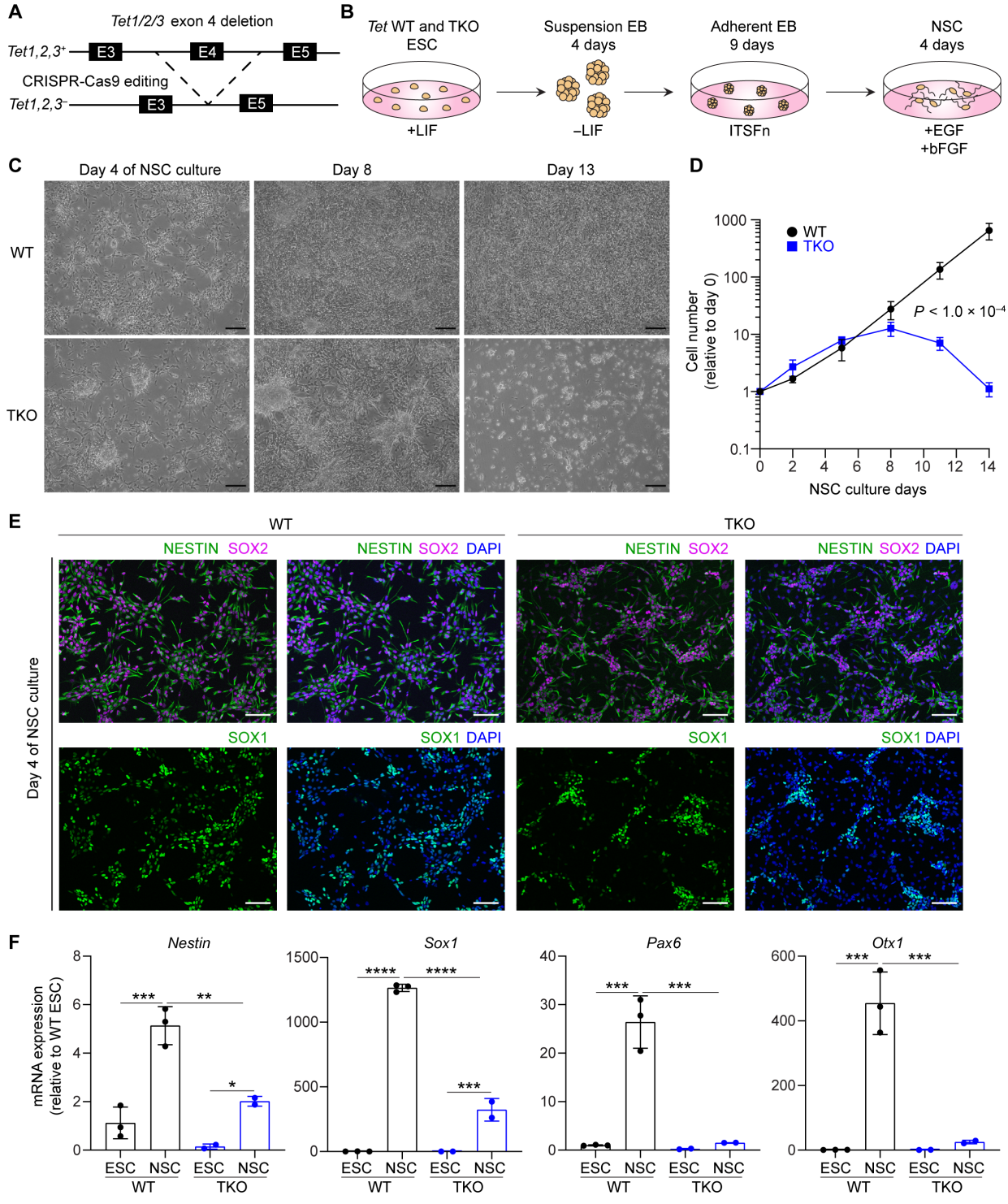

Fig. 1. *Tet* TKO NSCs derived from TKO ESCs have limited self-renewal and reduced expression of NSC markers. (**A**) Schematic of gene targeting strategy to delete exon 4 of *Tet1/2/3* and generate *Tet* TKO ESCs. (**B**) Overview of differentiation protocol for specification of NSCs from ESCs. EGF, epidermal growth factor. (**C**) Bright-field images of WT and TKO NSCs at days 4, 8, and 13 in culture (days after specification from ESCs). Scale bars, 100 μm. (**D**) Growth curve of WT and TKO NSCs over 2 weeks in culture. Cell numbers for each time point were plotted relative to cell numbers at day 0. Data represent means ± SD. Statistical significance assessed by two-way analysis of variance (ANOVA). Data represent three independent experiments. (**E**) Expression of NSC markers in WT and TKO NSCs assessed by immunofluorescence at day 4 (passage 1). Top: NSCs are stained with anti-NESTIN and anti-SOX2 antibodies. Bottom: NSCs are stained with anti-SOX1 antibody. Nuclei are stained by 4′,6-diamidino-2-phenylindole (DAPI). Scale bars, 100 μm. (**F**) Expression of neural markers quantified by RT-qPCR in ESCs and in NSCs at day 4 (passage 1). Data were normalized to *Gapdh*. Data represent means ± SD. Statistical significance assessed by one-way ANOVA and corrected for multiple testing with the Holm-Sidak method. **P* < 0.05, ***P* < 0.01, ****P* < 0.001, and *****P* < 0.0001. In all experiments, three WT and two TKO ESC or NSC biological replicates were used.

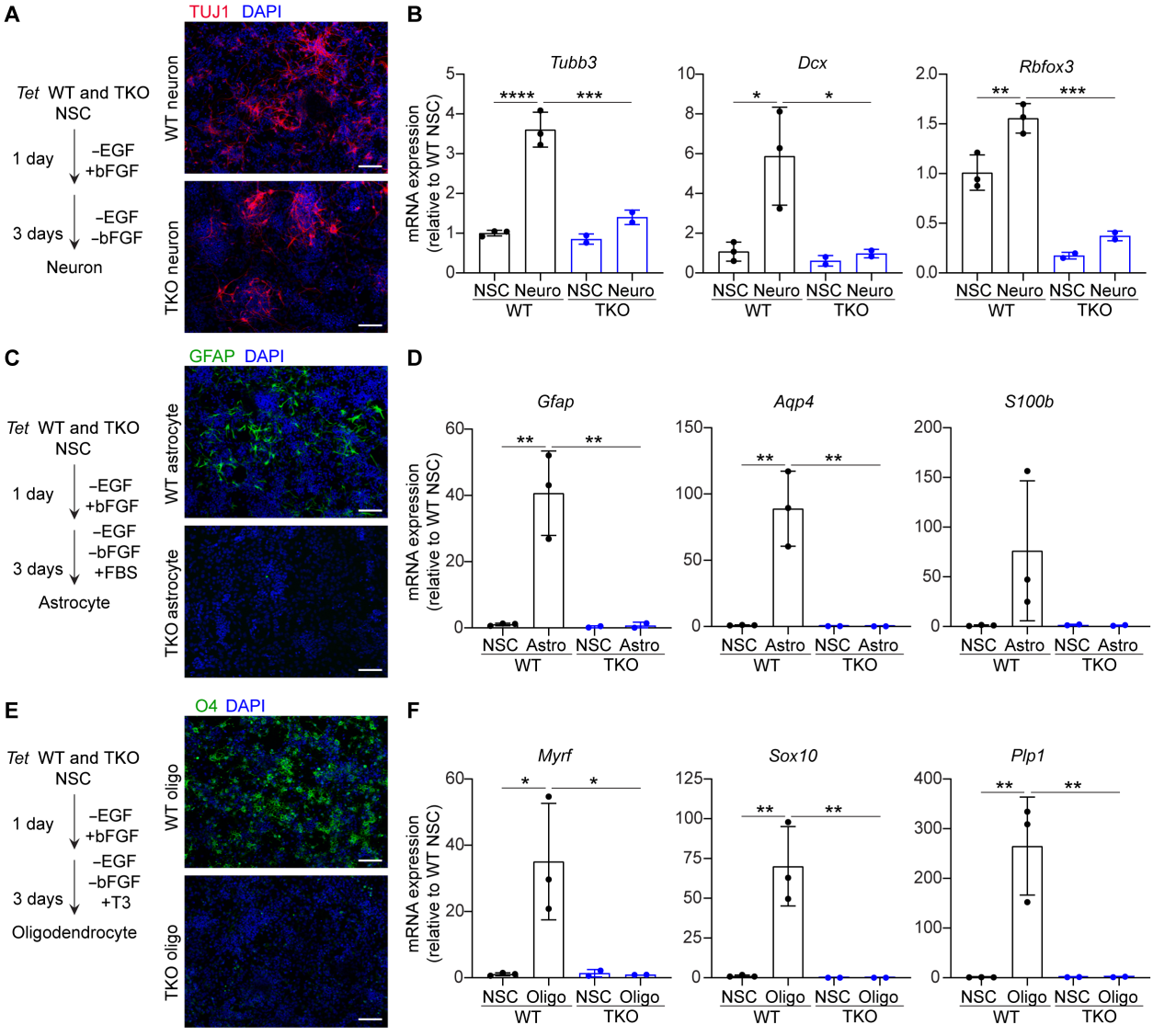

Fig. 2. *Tet* TKO NSCs retain neuronal competence but exhibit a severe block in glial differentiation. (**A**) WT and TKO NSCs are differentiated to neurons and stained with anti-TUJ1 on day 4 of differentiation. Nuclei are stained with DAPI. (**B**) Quantification of mRNA levels of neuronal markers in day 4 neuron (neuro) cultures and in NSCs by RT-qPCR. (**C**) WT and TKO NSCs are differentiated to astrocytes and stained with anti-GFAP on day 4 of differentiation. Nuclei are stained with DAPI. (**D**) Quantification of mRNA levels of astrocyte markers in day 4 astrocyte (astro) cultures and in NSCs by RT-qPCR. (**E**) WT and TKO NSCs are differentiated to oligodendrocytes (oligo) and stained with anti-O4 on day 4 of differentiation. Nuclei are stained with DAPI. (**F**) Quantification of mRNA levels of oligodendrocyte markers in day 4 oligodendrocyte cultures by RT-qPCR. For all experiments, three independent WT NSC lines and two independent TKO NSC lines were used. All lineage-specific differentiations were performed using passage 1 NSCs. All RT-qPCR data were normalized to *Gapdh*. Data represent means ± SD. Statistical significance was assessed by one-way ANOVA and corrected for multiple testing with the Holm-Sidak method. **P* < 0.05, ***P* < 0.01, ****P* < 0.001, and *****P* < 0.0001. Scale bars, 100 μm.

were previously identified as down-regulated by RT-qPCR (Fig. 1F) and are critical determinants of NSC identity, and other neural regulators such as *Emx2*, *Zic4*, *Lhx5*, *Rfx4*, and *Pou3f3*. However, of relevance to the glial differentiation block of TKO NSCs was the severe down-regulation of the *Nfia* family of glial TFs: *Nfia*, *Nfib*, and *Nfix* (Fig. 3E). Nuclear factor I A (NFIA) is required for the onset of astrocyte differentiation in the developing mouse spinal cord and is sufficient to confer glial competency onto human NSCs (*27*, *28*). In addition, individual knockout of *Nfia*, *Nfib*, or *Nfix* in mice results in loss of astroglia in the brain (*29*–*31*). We validated the reduced expression of *Nfia*, *Nfib*, and *Nfix* in TKO NSCs by RT-qPCR (Fig. 3F) and confirmed their failure to be induced upon differentiation of TKO NSCs into astrocytes (Fig. 3G), suggesting that their impaired expression may underlie the astrocytic differentiation defect. Likewise, we found the oligodendrocyte TFs *Olig1* and *Olig2* to be down-regulated in TKO NSCs (Fig. 3E). Both genes are required for oligodendrocyte development (*32*, *33*), making them attractive candidates to explain the oligodendrocyte differentiation defect of TKO NSCs. Last, key genes defining the radial glial state of NSCs, such as *Slc1a3* and *Fabp7* (*34*), were also down-regulated in TKO NSCs (Fig. 3E), suggesting that TKO NSCs were impaired in adopting a radial glial identity and may remain in a more primitive neuroepithelial

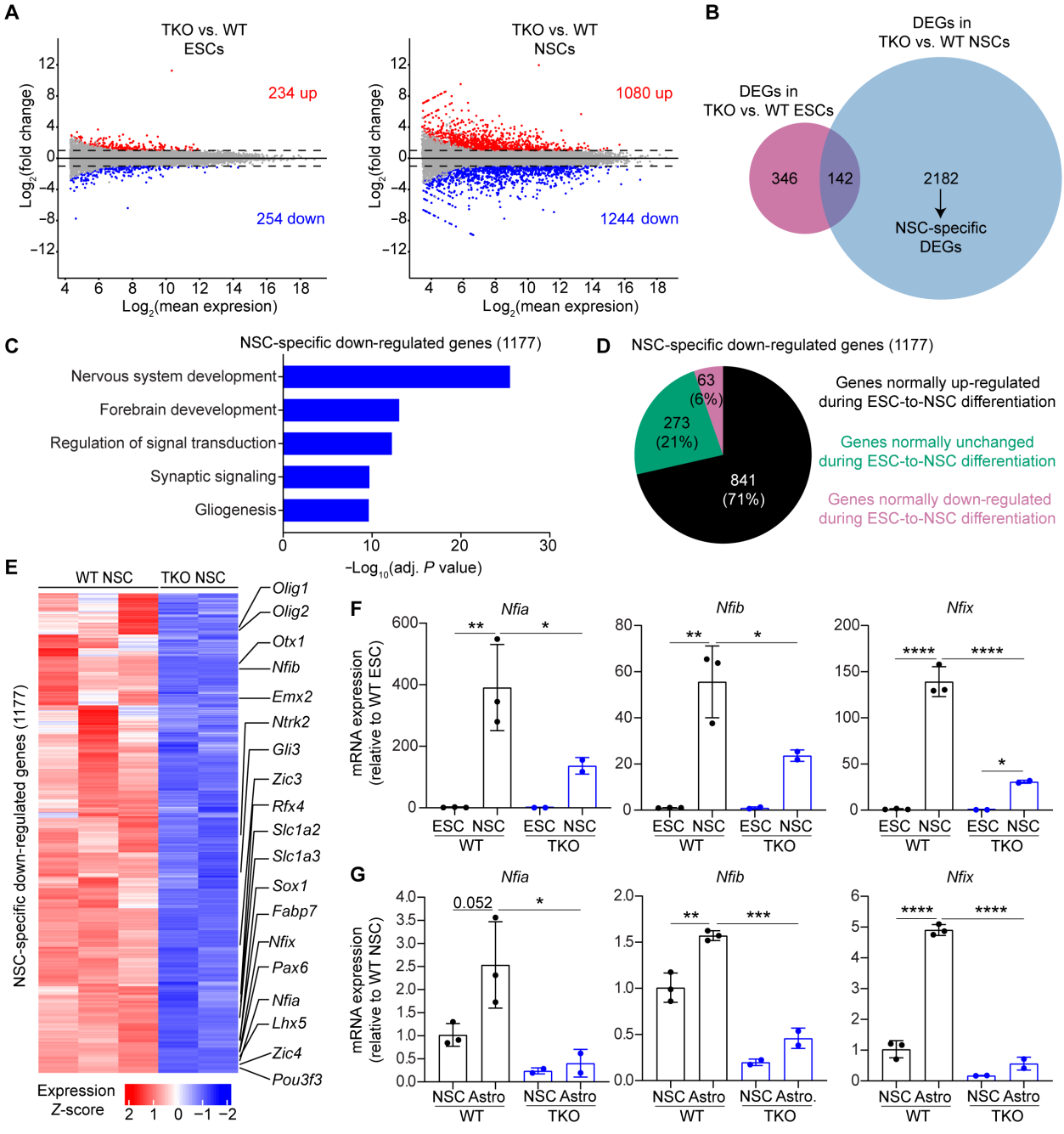

Fig. 3. Neurodevelopmental and glial gene expression programs are severely impaired in *Tet* TKO NSCs. (**A**) MA plots of gene expression changes in TKO versus WT ESCs (left) and in TKO versus WT passage 1 NSCs (right) as quantified by RNA-seq. DEGs are shown in red (up-regulated) and blue (down-regulated). DEGs were defined by |fold change| ≥ 2 and false discovery rate (FDR) ≤ 0.05. Data represent three WT and two TKO biological replicates per cell type. (**B**) Venn diagram displaying intersection of DEGs in TKO versus WT ESCs and DEGs in TKO versus WT NSCs. Note the 2182 genes uniquely affected in NSCs. (**C**) Representative gene ontology (GO) terms for the top 5 annotation categories among NSC-specific down-regulated genes. (**D**) NSC-specific down-regulated genes in TKO NSCs are classified into those that are up-regulated, down-regulated, or unchanged during differentiation of WT ESCs to WT NSCs. (**E**) Heatmap displaying *z*-scores of normalized expression of NSC-specific down-regulated genes in TKO NSCs. Key neurodevelopmental and glial genes are annotated. (**F**) Quantification of mRNA levels of *Nfi* family genes in ESC and NSC cultures by RT-qPCR. (**G**) Quantification of mRNA levels of *Nfi* family genes in NSC and astrocyte cultures by RT-qPCR. All RT-qPCR data represent means ± SD. Statistical significance was assessed by one-way ANOVA and corrected for multiple testing with the Holm-Sidak method. **P* < 0.05, ***P* < 0.01, ****P* < 0.001, and *****P* < 0.0001.

state. Together, these findings demonstrate a failure to properly induce neurodevelopmental gene expression programs in the absence of TET enzymes during NSC specification, especially those governing the glial differentiation capacity and radial glial identity of NSCs.

Regions undergoing TET-mediated developmental DNA demethylation during NSC specification have features of enhancers and are associated with neural and glial genes

To identify regions undergoing TET-dependent demethylation during NSC differentiation, we performed genome-wide methylation profiling of WT and TKO ESCs and NSCs by whole-genome bisulfite sequencing (WGBS). We found that global methylation at CpG dinucleotides was increased by ~10% between ESC and NSC states, with TKO ESC and NSCs exhibiting 1 to 3% higher methylation levels compared to WT cells (fig. S3A). Next, we identified differentially methylated regions (DMRs), which were defined as regions containing at least five CpGs with a total methylation level difference of at least 20% and false discovery rate (FDR) of less than 0.05. Consistent with the demethylation function of TET enzymes, the vast majority of DMRs identified between TKO and WT ESCs or NSCs was hypermethylated (Fig. 4A). We identified 11,489 hyperDMRs between TKO and WT ESCs and 7203 hyperDMRs between TKO and WT NSCs (which, after excluding regions that were hypermethylated in TKO ESCs, yielded 5647 NSC-unique hyperDMRs). To determine which of these hypermethylated regions are of developmental significance in NSC specification, we first sought to identify regions that normally undergo demethylation during the ESC-to-NSC transition. To this end, we identified DMRs between WT ESCs and WT NSCs, which revealed 27,462 hypermethylated and 4332 hypomethylated regions (Fig. 4A, middle bar). We term the latter 4332 regions developmental hypoDMRs. These regions were of particular interest as they might shed light on the functional role of developmental demethylation in NSC specification. We next assessed how deficiency of TET enzymes affects the methylation status of these developmentally demethylated regions. Seventy-six percent of developmental hypoDMRs (3294 of 4332) were hypermethylated in TKO cells (Fig. 4B), revealing that the majority of developmental demethylation during NSC specification is TET dependent. We termed these regions NSC TKO devDMRs. All other DMRs in TKO NSCs that were not developmentally demethylated during normal NSC specification were termed NSC TKO non-devDMRs (fig. S3B).

The NSC TKO devDMRs, in contrast to NSC non-devDMRs or TKO ESC DMRs, had several unique features: (i) NSC TKO devDMRs exhibited the greatest average increase in methylation between TKO and WT cells (Fig. 4C and fig. S3C), suggesting that hypermethylation at these sites could have especially prominent effects. (ii) A significantly greater fraction of NSC TKO devDMRs (79.17%) were in introns and intergenic regions compared to ESC TKO DMRs (52.39%, $P < 2.2 \times 10^{-16}$) and NSC TKO non-devDMRs (52.49%, $P < 2.2 \times 10^{-16}$) (Fig. 4D). Likewise, a significantly smaller fraction of NSC TKO devDMRs (13.20%) were at promoter regions compared to ESC TKO DMRs (35.56%, $P < 2.2 \times 10^{-16}$) and NSC TKO non-devDMRs (40.14%, $P < 2.2 \times 10^{-16}$) (Fig. 4D). These notable differences in genomic annotations support the possibility that NSC TKO devDMRs may contain a higher proportion of nonpromoter cis-regulatory elements. (iii) Genes associated with NSC TKO devDMRs were highly enriched for NSC-specific down-regulated genes compared to genes associated with ESC TKO DMRs and NSC TKO non-devDMRs (Fig. 4E). Several neurodevelopmental regulators including *Sox1*, *Pax6*, *Otx1*, *Emx2*, *Zic4*, *Lhx5*, *Rfx4*, and *Pou3f3* as well as glial TF genes *Nfia*, *Nfib*, *Nfix*, *Olig1*, and *Olig2* were among the down-regulated genes in NSCs that were associated with NSC TKO devDMRS (data S1). This suggests that loss of TET function at NSC TKO devDMRs may underlie a large proportion of the impaired gene expression we observe in TKO NSCs. (iv) Last, sequence conservation of NSC TKO devDMRs across 60 vertebrate species was higher than conservation of ESC TKO DMRs or NSC TKO non-devDMRs, suggesting that they may contain the greatest proportion of regions with prominent gene-regulatory significance (Fig. 4F). Together, these features suggest that regions undergoing TET-dependent demethylation during NSC specification (i.e., NSC TKO devDMRs) may represent conserved cis-regulatory elements and that loss of demethylation at these sites may contribute to the impaired induction of neurodevelopmental genes in TKO NSCs.

To gain further insight into potential gene regulatory functions of NSC TKO devDMRs, we performed motif enrichment analysis to identify candidate TFs with sequence specificity in these regions. We found many SOX TFs to be highly enriched, including the master regulators of NSC identity SOX2/3, oligodendrocyte development factor SOX10, and glial cell fate determinant SOX9 (Fig. 4G). Using published SOX2, SOX3, and SOX9 occupancy datasets in neural progenitor cells (*35*) and glial progenitor cells (*36*), we confirmed robust enrichment of these TFs at hundreds of NSC TKO devDMRs (fig. S3D), which further supports regulatory roles for these regions. In addition, leveraging publicly available WGBS datasets from the ENCODE consortium (*37*), we observed that NSC TKO devDMRs had lower levels of DNA methylation in E11.5 mouse neural tissues relative to flanking regions and nonneural tissues, suggesting that these regions are hypomethylated in vivo and that their hypomethylation is mostly neural specific (Fig. 4H). We also found that the NSC TKO devDMRs had higher levels of H3 lysine-27 acetylation (H3K27ac), a mark associated with active enhancers, in neural compared to nonneural tissues (Fig. 4I). Consistently, 97 NSC TKO devDMRs overlapped enhancers with regulatory activity in mouse E11.5 embryos as reported by the VISTA Enhancer Browser ($P = 1.0 \times 10^{-3}$, 10^3 permutation tests) (Fig. 4J) (*38*). A large fraction of them (80 of 97, enrichment $P = 5.7 \times 10^{-14}$) drove expression in neural tissues and included devDMRs in proximity to NSC-specific down-regulated genes with prominent neurodevelopmental roles (Fig. 4J and fig. S3, E and F). The TKO NSC devDMRs in proximity to the glial TF genes *Nfia*, *Nfib*, and *Nfix* were in highly conserved regions and marked by H3K27ac in mouse E11.5 forebrain (Fig. 4K). Last, using a previously published CCCTC-binding factor (CTCF) chromatin immunoprecipitation sequencing (ChIP-seq) dataset from mouse NSCs (*39*), we assessed CpG methylation levels at 42,890 CTCF-binding sites. No difference in methylation was observed between WT and TKO NSCs (fig. S3G). A mere 133 (0.31%) of the 42,890 CTCF peaks were located at NSC TKO devDMRs (fig. S3H), largely excluding CTCF sites as major targets of TET-dependent demethylation. Together, these findings suggest that NSC TKO devDMRs are likely located at enhancers and their DNA methylation status may influence neural enhancer activity and expression of key neurodevelopmental and glial TF genes.

TET-mediated DNA demethylation is essential for neural enhancer establishment and activation during specification of NSCs

To examine whether NSC TKO devDMRs are located at neural enhancers and affect enhancer chromatin states, we mapped the

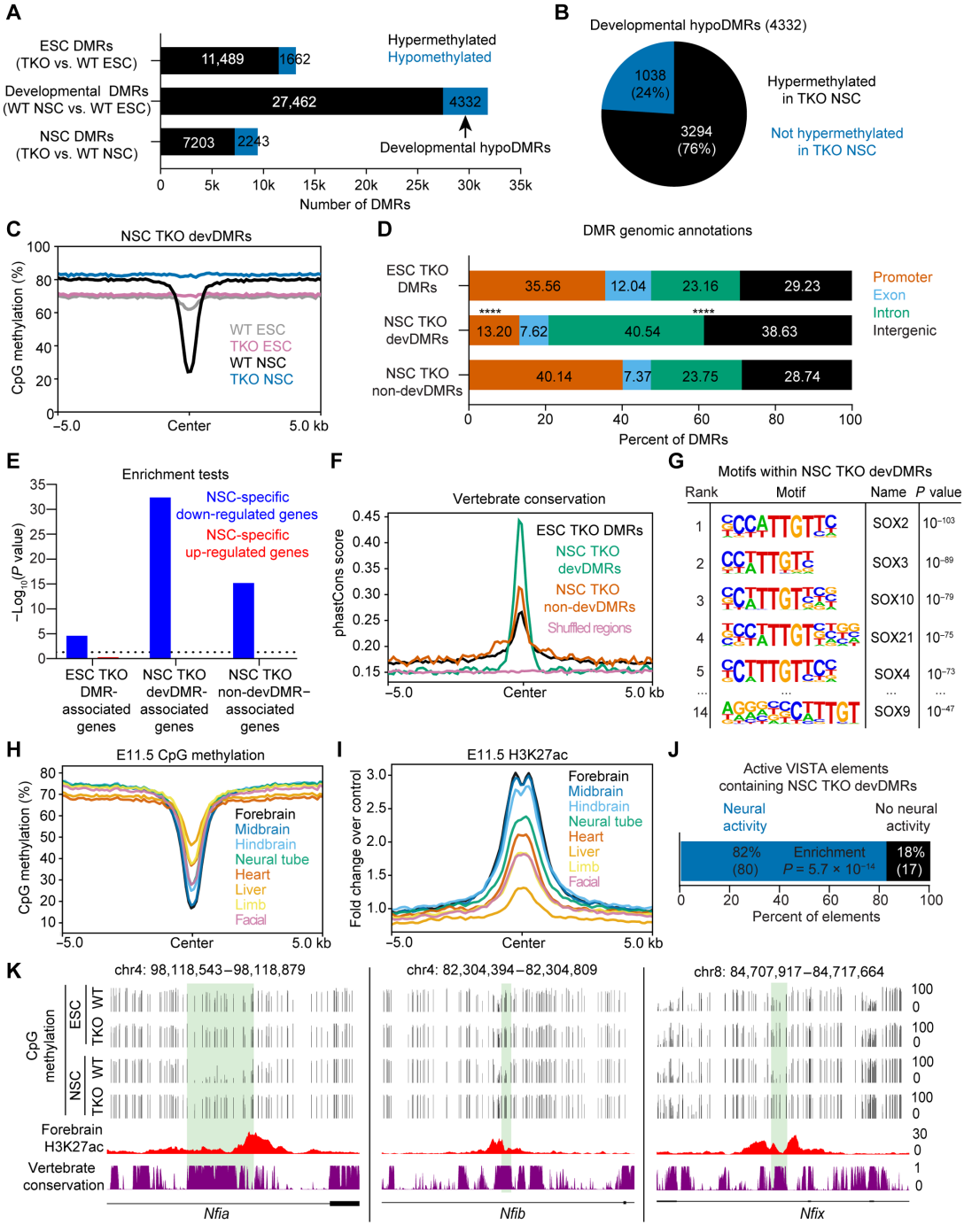

Fig. 4. Regulatory elements displaying enhancer features undergo *Tet*-dependent DNA demethylation during ESC-to-NSC differentiation. (**A**) Numbers of DMRs identified by WGBS in TKO versus WT ESCs, WT NSC versus WT ESC (i.e., developmental DMRs), and TKO versus WT NSCs are plotted. DMRs were defined as regions with a minimum of five CpGs, average methylation difference of at least 20%, and an FDR of ≤0.05. Passage 1 NSCs were used for WGBS analyses. Data represent one WT and one TKO biological replicate per cell type. (**B**) Fraction of developmental hypoDMRs that are hypermethylated in TKO NSCs. (**C**) Average CpG methylation at ±5 kb from the center of the NSC TKO devDMRs in WT and TKO ESCs and NSCs. (**D**) Annotation of DMRs to genomic regions. Statistical significance was assessed by the two-proportion *z* test. ****$P < 2.2 \times 10^{-16}$. (**E**) Statistical enrichment of DMR-associated genes for NSC-specific DEGs as determined by the hypergeometric test. Plotted values are $-\log_{10}(P$ value). Dotted line indicates $-\log_{10}(0.05)$. (**F**) Average phastCons scores for the indicated DMR classes and shuffled genomic regions. (**G**) Top: TF motifs enriched among NSC TKO devDMRs determined by HOMER known motif analysis. (**H**) Average CpG methylation at NSC TKO devDMRs in E11.5 mouse tissues. Methylation data were obtained from the ENCODE consortium. (**I**) Average H3 lysine-27 acetylation (H3K27ac) at NSC TKO devDMRs in E11.5 mouse tissues. H3K27ac data were obtained from the ENCODE consortium. (**J**) Proportion of active VISTA elements containing an NSC TKO devDMR with nervous system activity. Data were obtained from the VISTA Enhancer Browser. Enrichment *P* value was calculated with the hypergeometric test. (**K**) Genome browser tracks displaying CpG methylation, E11.5 forebrain H3K27ac from ENCODE, and vertebrate conservation phastCons scores at introns of *Nfi* family genes where representative NSC TKO devDMRs are highlighted in green.

genome-wide distribution of histone H3 lysine-4 monomethylation (H3K4me1) and H3K27ac in WT and TKO ESCs and NSCs by cleavage under targets and tagmentation (CUT&Tag). Deposition of H3K4me1 during cell state transitions indicates enhancer establishment, which precedes the addition of H3K27ac (*40*). The co-occurrence of the two marks is a well-established indicator of active enhancers (*41*). The global levels of both histone marks were reproducible between biological replicates of each cell type and genotype (fig. S4A). We found that the levels of H3K4me1 and H3K27ac at NSC TKO devDMRs were very low in ESCs. However, upon differentiation to NSCs, their levels markedly increased at these regions, suggesting adoption of an active chromatin state (Fig. 5A). In TKO NSCs, the levels of both marks were reduced to approximately half in these regions ($P < 2.2 \times 10^{-16}$ for both marks) (Fig. 5A), suggesting that failure of TET-dependent developmental demethylation may have impaired proper deposition of H3K4me1 and H3K27ac. This indicates a potential role for TET-dependent demethylation in commissioning enhancers during NSC specification.

To better understand how developmental demethylation affects the establishment and activation of neural-specific enhancers during specification of NSCs from ESCs, we first identified active enhancers [H3K4me1$^+$ H3K27ac$^+$, > 2 kb from transcriptional start site (TSS)] in both cell types. By excluding active enhancers shared between WT ESCs and NSCs, we obtained a set of 4347 enhancers unique to NSCs (Fig. 5B). A significant fraction of NSC-unique enhancers (784, $P = 1.0 \times 10^{-3}$) contained an NSC TKO devDMR (Fig. 5B). A total of 53.3% (418 of 784) of these enhancers had significantly reduced levels of H3K4me1 and H3K27ac in TKO cells [$\log_2$(fold change) < 0, $P < 0.05$], compared to only 1.1% (9 of 784) that had increased levels of both marks [$\log_2$(fold change) > 0, $P < 0.05$] (Fig. 5C). Levels of H3K27ac were highly correlated with levels of H3K4me1 (adjusted $R^2 = 0.7453$) (Fig. 5C), indicating that derangement of these marks was likely due to a common process. This supports an overwhelming failure to establish and activate NSC-specific enhancers in the absence of TET-dependent demethylation. Although 43% of all NSC-unique enhancers had lower levels of both H3K4me1 and H3K27ac in TKO NSCs (fig. S4B), the levels of these marks at enhancers with a devDMR were significantly lower than those at enhancers without a devDMR (Fig. 5D). The number of active enhancers with NSC TKO devDMRs and loss of H3K4me1 and H3K27ac was significantly greater than expected by chance (enrichment $P = 1.75 \times 10^{-9}$). The number of active enhancers with NSC TKO devDMRs and gain of both marks was significantly less than expected by chance (depletion $P = 1.30 \times 10^{-8}$) (Fig. 5C). This further supports that DNA hypermethylation affects enhancer commissioning. NSC TKO devDMR–associated enhancers that had reduced levels of both histone marks were associated with 80 NSC-specific DEGs, most of which were down-regulated and included neural regulators *Sox1*, *Rfx4*, *Pou3f3*, *Gli3*, and *Ntrk2* as well as glial TFs *Nfia*, *Olig1*, and *Olig2* (Fig. 5, E and F, and fig. S4C). Last, given that some NSC active enhancers exist in a poised state in ESCs (H3K4me1$^+$ H3K27ac$^-$) and become active upon differentiation (*41*), we assessed whether TET-dependent demethylation affected activation of ESC poised enhancers. Of the 784 NSC-unique active enhancers with NSC TKO devDMRs, 123 (15.7%) were poised in ESCs, indicating that most NSC enhancers targeted by TETs for demethylation are established de novo in NSCs (661, 84.3%). Notably, most of the ESC poised–NSC active enhancers with NSC TKO devDMRs exhibited loss of H3K4me1, H3K27ac, or both (fig. S4D), indicating that TET-dependent demethylation is required for the sustained commissioning of these enhancers. Notably, a decommissioned enhancer in proximity to *Sox1* (fig. S4C) was poised in the ESC state, suggesting that deregulation of ESC poised enhancers by loss of demethylation negatively affects general neurodevelopmental programs. Together, these findings suggest that lack of TET-dependent developmental demethylation during NSC specification significantly impairs establishment and activation of enhancers of neural and glial TF genes, underpinning a TET-dependent establishment of NSC identity and gliogenic potential.

We next assessed the effect of TET loss on poised enhancers unique to the NSC state (H3K4me1$^-$ H3K27ac$^-$ in ESCs and H3K4me1$^+$ H3K27ac$^-$ in NSCs). By excluding ESC poised enhancers, we obtained a set of 13,846 poised enhancers unique to the NSC stage. A total of 1111 NSC-unique poised enhancers contained an NSC TKO devDMR ($P = 1.0 \times 10^{-3}$) (Fig. 5B). NSC-unique poised enhancers with devDMRs displayed significantly lower levels of H3K4me1 than enhancers without devDMRs (fig. S4E). Of the 1111 NSC-unique poised enhancers with a devDMR, the majority (690, 62%) exhibited significantly reduced H3K4me1 [$\log_2$(fold change) < 0, $P < 0.05$], a number significantly greater than expected by chance (enrichment $P = 1.88 \times 10^{-41}$). In contrast, only 36 (3%) of NSC-unique poised enhancers with a devDMR exhibited significantly increased H3K4me1 [$\log_2$(fold change) < 0, $P < 0.05$], significantly fewer than expected by chance (depletion $P = 3.45 \times 10^{-34}$) (fig. S4F). Genes associated with NSC-unique poised enhancers with devDMRs and loss of H3K4me1 were highly enriched for neurodevelopmental processes including gliogenesis (fig. S4G). These findings indicate that loss of TET-mediated demethylation during NSC specification compromises the commissioning of NSC poised enhancers and may negatively affect the expression of proximal glial and neuronal genes upon NSC differentiation.

Loss of TET-mediated developmental DNA demethylation compromises enhancer-promoter interactions at glial genes

To assess whether TET-dependent demethylation of glial enhancers was required for interaction of these enhancers with their target gene promoters, we performed promoter-capture high-throughput chromosome conformation capture (HiC) on WT and TKO NSCs. We found ~60,000 total promoter-interacting chromatin loops in each WT and NSCs (Fig. 6A). Assessment of differential loops between WT and TKO NSCs based on loss or gain of one or both loop anchors revealed that 41,345 loops were lost and 39,876 loops were gained in TKO NSCs, indicating extensive reconfiguration of promoter contacts in the absence of TET enzymes (Fig. 6B). A total of 307 loops between promoters and the enhancers that contained NSC TKO devDMRs were lost in TKO NSCs, while 165 loops were gained (Fig. 6C). Most (182 of 307, 59%) of the lost enhancer-promoter contacts were also associated with loss of enhancer H3K4me1 and H3K27ac (Fig. 6C), suggesting that failure to commission enhancers in the absence of TET-dependent DNA demethylation is accompanied by failure to contact target gene promoters. Many loops between the promoters of critical glial genes and TET-demethylated enhancers were lost in TKO NSCs. For example, TET-demethylated enhancers with impaired commissioning failed to contact the promoters of oligodendrocyte TFs *Olig1* and *Olig2* (Fig. 6D), master glial TF *Sox9* (Fig. 6E), and radial glial identity gene *Fabp7* (fig. S5A). At the *Nfia* locus, we observed displacement of a loop anchor 42 kb away from its normal contact site at a TET-demethylated enhancer (fig. S5B), suggesting that enhancer hypermethylation can misdirect loop formation as well. Together, these results indicate that loss of TET-dependent DNA demethylation at enhancers during NSC specification compromises the proper wiring of enhancer-promoter interactions at glial genes and likely contributes to loss of TKO NSC gliogenic competence.

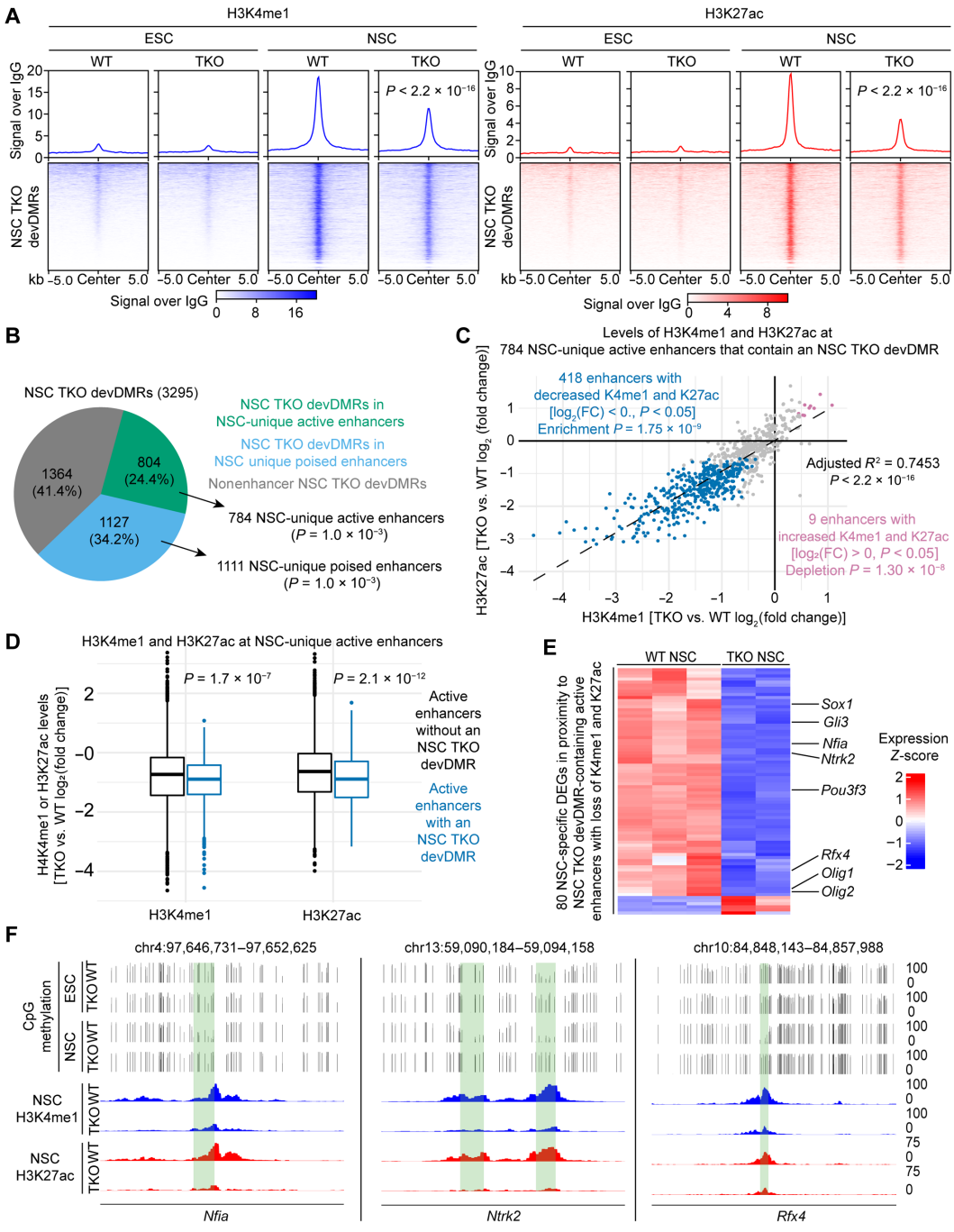

Fig. 5. NSC TKO devDMRs are associated with loss of enhancer commissioning in proximity to neurodevelopmental and glial genes. (**A**) Profile plots (top) and heatmaps (bottom) displaying H3K4me1 (left) and H3K27ac (right) levels at NSC TKO devDMRs as profiled by CUT&Tag in WT and TKO ESCs and passage 1 NSCs. Data represent two WT and TKO biological replicates per cell type. Statistical significance assessed by Student's *t* test. (**B**) Pie chart displaying proportion of NSC TKO devDMRs falling into NSC-unique active enhancers (green) and NSC-unique poised enhancers (blue). Statistical significance of DMR and enhancer overlaps on the basis of 10^3 random permutations. (**C**) Fold change of H3K4me1 and H3K27ac between TKO and WT NSCs at the 784 NSC-unique enhancers that contain an NSC TKO devDMR. Enhancers with significantly reduced H3K4me1 and H3K27ac [$\log_2$(fold change) < 0, $P < 0.05$] are in blue. Enhancers with significantly increased H3K4me1 and H3K27ac [$\log_2$(fold change) > 0, $P < 0.05$] are in red. Enrichment and depletion *P* values were computed by hypergeometric tests. FC, fold change. (**D**) Comparison of mean H3K4me1 (left) and H3K27ac (right) levels between NSC-unique active enhancers with and without an NSC TKO devDMR. Values plotted are $\log_2$(fold change) of TKO versus WT. Statistical significance computed with Student's *t* test. (**E**) Heatmap of expression of NSC-specific DEGs that are in proximity to NSC-unique active enhancers that contain an NSC TKO devDMR and have lost H3K4me1 and H3K27ac in TKO NSCs. Heatmap displays *z*-scores of normalized expression. Notable neurodevelopmental and glial genes are noted. (**F**) Genome browser tracks displaying DNA methylation and H3K4me1 and H3K27ac CUT&Tag signals at NSC TKO devDMR-containing NSC-unique active enhancers in introns of selected neural genes. Note the reduced levels of H3K4me1 and H3K27ac at these regions in TKO NSCs. NSC TKO devDMRs are highlighted in green. CUT&Tag tracks display immunoglobulin G (IgG)–subtracted signal.

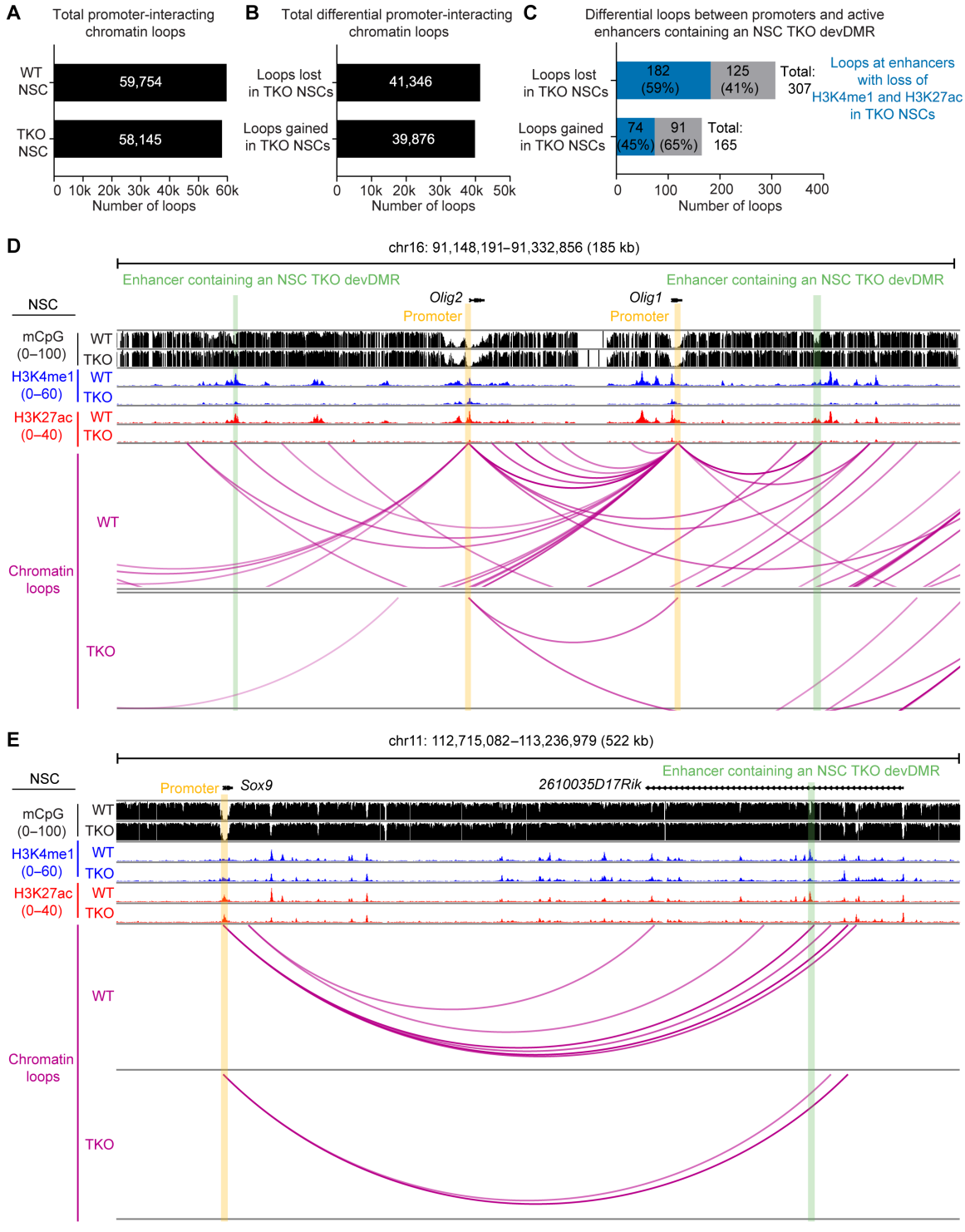

Fig. 6. Loss of TET-mediated developmental DNA demethylation compromises enhancer-promoter interactions at glial genes. (**A**) Total promoter-interacting chromatin loops in WT and TKO NSCs identified by promoter-capture HiC. (**B**) Total promoter-interacting loops lost and gained in TKO NSCs based on loss or gain of one or both loop anchors. (**C**) Loops lost and gained in TKO NSCs between promoters and active enhancers containing an NSC TKO devDMR. The number of loops in blue indicates loops associated with enhancers that have loss of H3K4me1 and H3K27ac in TKO NSCs. (**D**) Genome-browser view of the *Olig1/2* locus. Note the loss of the interactions between TET-demethylated enhancers with impaired commissioning and the promoters of *Olig1* and *Olig2*. Green indicates enhancers containing an NSC TKO devDMR. Orange indicates promoter regions. (**E**) Genome-browser view of the *Sox9* locus. Note the loss of the interaction between the TET-demethylated enhancer with impaired commissioning and the *Sox9* promoter. Green indicates enhancers containing an NSC TKO devDMR. Orange indicates promoter regions.

Restoring TET demethylase activity is sufficient to ameliorate reduced neural gene expression and rescue the self-renewal and gliogenic defects of TKO NSCs

To validate that TET-dependent demethylation is required for establishment of NSC identity and gliogenic competence, we expressed WT or enzymatically dead TET1 catalytic domain (*Tet1CD*) in TKO ESCs and differentiated them to NSCs (Fig. 7A). Expression of WT *Tet1CD*, but not the mutant form, ameliorated the reduced expression of *Pax6* and *Otx1* (Fig. 7B) and robustly restored self-renewal of TKO NSCs (Fig. 7C). When differentiated to astrocytes, TKO NSCs transduced with WT *Tet1CD* were able to form GFAP$^+$ astrocytes, while those transduced with empty or mutant vectors could not

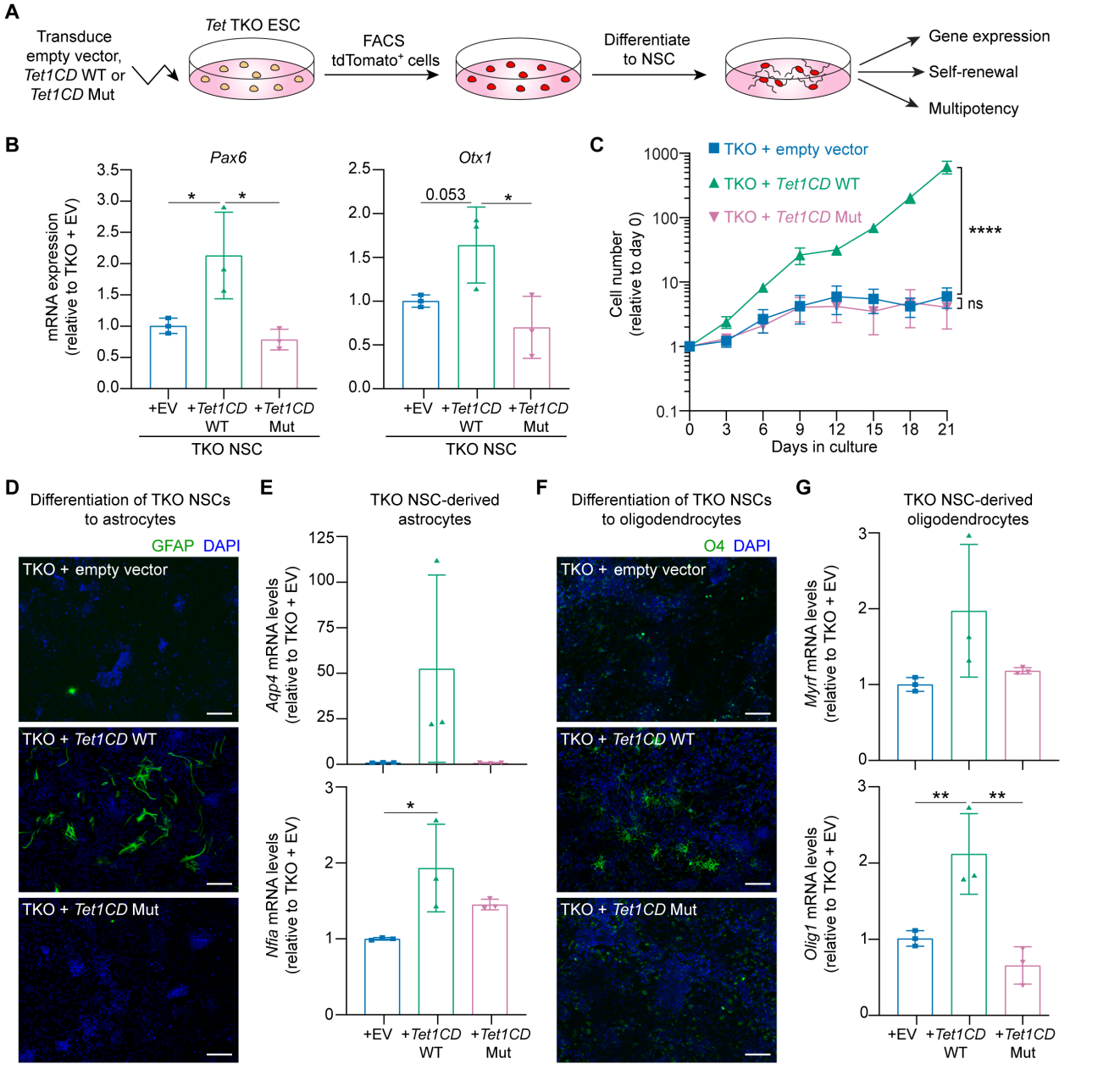

Fig. 7. Rescue of TKO NSC neural gene expression, self-renewal, and multipotency by TET catalytic activity. (**A**) Schematic of experiments to rescue TKO NSC phenotypes by restoring TET catalytic activity. Mut, mutant. (**B**) *Pax6* and *Otx1* mRNA levels quantified by RT-qPCR in passage 1 NSCs. EV, empty vector. (**C**) Growth curve of TKO NSCs over 3 weeks in culture. Cell numbers for each time point were plotted relative to cell numbers at day 0. Data represent means ± SD. Statistical significance assessed by two-way ANOVA. ****$P < 0.0001$. ns, not significant. (**D**) TKO NSCs are differentiated to astrocytes and stained with anti-GFAP on day 4 of differentiation. Nuclei are stained with DAPI. Scale bars, 100 μm. (**E**) Quantification of mRNA levels of astrocyte markers in day 4 astrocyte cultures by RT-qPCR. (**F**) TKO NSCs are differentiated to oligodendrocytes and stained with anti-O4 on day 4 of differentiation. Nuclei are stained with DAPI. Scale bars, 100 μm. (**G**) Quantification of mRNA levels of oligodendrocyte markers in day 4 oligodendrocyte cultures by RT-qPCR. For all panels, data represent three independent experiments. For (B), (E), and (G), data represent means ± SD. Statistical significance was assessed by one-way ANOVA and corrected for multiple testing with the Holm-Sidak method. *$P < 0.05$ and **$P < 0.01$.

(Fig. 7D). These astrocytes expressed higher levels of *Aqp4* and *Nfia* compared to controls (Fig. 7E). Likewise, TKO NSCs transduced with WT *Tet1CD* were able to form $O4^+$ oligodendrocytes, while those transduced with empty or mutant vectors could not (Fig. 7F). These oligodendrocytes expressed higher levels of *Myrf* and *Olig1* compared to controls (Fig. 7G). These findings demonstrate that the acquisition of NSC identity and gliogenic competence depend on TET enzymatic activity and underscore the significance of TET-dependent demethylation during NSC differentiation.

Loss of TET enzymes in mouse dorsal telencephalic NSCs impairs glial gene expression and results in neurodevelopmental defects

To investigate the effects of TET loss on gliogenesis and mouse cortical development, we conditionally deleted all three *Tet* genes in dorsal telencephalic NSCs using the $Emx1^{Cre}$ mouse strain, which induces recombination by E10.5 (*42*). The dorsal telencephalon is the embryonic primordium of structures including the neocortex and hippocampus. As cortical gliogenesis is largely a late embryonic and postnatal process, conditional deletion of *Tet1/2/3* at midgestation permits the study of TET loss on NSC gliogenic potential in vivo. We mated male $Emx1^{+/Cre};Tet1^{+/f};Tet2^{+/f};Tet3^{+/-}$ mice with female $Emx1^{+/+};Tet1^{f/f};Tet2^{f/f};Tet3^{f/f}$ mice to obtain $Emx1^{+/Cre};Tet1^{f/f};Tet2^{f/f};Tet3^{f/-}$ mice, which are hereafter referred to as conditional TKO (cTKO) mice (fig. S6A). *Tet* cTKO mice were produced at the expected proportion on postnatal day 21 (P21) (fig. S6B), indicating that loss of TET enzymes in dorsal telencephalic NSCs is compatible with embryonic and early postnatal development. We confirmed that all floxed alleles were successfully recombined in P21 cortical tissue but not in neural tissues outside of the $Emx1^{Cre}$ expression zone such as the cerebellum, eye, and spinal cord (fig. S6C), confirming highly efficient and specific recombination of *Tet* genes by $Emx1^{Cre}$ in the cortex. *Tet* cTKO mice were comparable to littermate controls in weight at birth (P0) but became runted in the first weeks of life, were severely underweight by P21 (fig. S6D), and died around 1 month of age (fig. S6E). Their brains appeared morphologically normal but were slightly smaller and weighed less than the brains of control mice (fig. S6, F and G). These results indicate that midgestational loss of TET enzymes in dorsal telencephalic NSCs does not categorically prevent corticogenesis but leads to postnatal lethality. Histological examination of cTKO brains revealed two notable defects. First, while the corpus callosum (indicated by arrows) was observed at the level of the lateral ventricles in cTKO brains (Fig. 8A, left), it was absent at the level of the dorsal hippocampus and medial/lateral habenulas (Fig. 8A, middle). Second, the hippocampus of cTKO brains was notably smaller compared to controls, particularly the dentate gyrus (indicated by arrowheads), which was severely underdeveloped (Fig. 8A, middle and right). This indicates that TET enzymes are required for proper development of the corpus callosum and hippocampus.

To examine the cell composition of cTKO brains, we stained cortical sections with markers of neurons, oligodendrocytes, and astrocytes. Neuronal nuclear antigen $(NEUN)^+$ neurons were abundantly detected throughout the hippocampus and cortex of control and cTKO brains (Fig. 8B and fig. S7A), indicating that neurogenesis largely remained intact. $OLIG2^+$ oligodendrocytes were also present in control and cTKO brains, indicating that oligodendrocytes can develop upon loss of TETs (fig. S7B). However, myelin component MBP (myelin basic protein) was markedly reduced, suggesting an impairment in oligodendrocyte function (fig. S7B). $GFAP^+$ astrocytes were abundant in control hippocampi but were virtually absent in cTKO hippocampi (Fig. 8B). GFAP expression was also lost in venous sinus–associated cells (fig. S7A). However, staining hippocampal sections for astrocyte marker aquaporin 4 (AQP4) revealed comparable expression between control and cTKO brains (fig. S7C), indicating that astrocyte development is not completely blocked upon TET loss in dorsal telencephalic NSCs but rather that astroglial gene expression is compromised.

To examine whether the morphological abnormalities and astroglial gene expression defects observed in postnatal cTKO brains manifested during embryogenesis, we stained E17.5 cTKO brains for neuronal, glial, and NSC markers. NEUN staining revealed the hippocampal dentate gyrus to be underdeveloped in cTKO embryos (Fig. 8C), indicating that this defect arises during gestation. GFAP expression was lost from the hippocampal ventricular zone of cTKO brains (Fig. 8D), but NSC marker SOX2 was abundantly detected there (fig. S7D), suggesting that NSCs remain intact upon loss of TET enzymes but that their adoption of a radial glial identity is partially compromised. This is consistent with the down-regulation of radial glial markers in TKO NSCs, including *Slc1a3* and *Fabp7* (Fig. 3E), as well as with their altered neural TF repertoire and loss of glial competence. Last, given the partial absence of the corpus collosum in cTKO mice, we examined the formation of the glial wedge, a midline glial structure important for axon guidance and corpus callosum development (*43*). The glial wedge was absent in cTKO brains based on staining for GFAP (fig. S7D). These results affirm an embryonic origin for the neuroanatomic defects observed in P21 brains and support a role for TET enzymes in establishing proper glial gene expression during embryonic neurodevelopment.

DISCUSSION

DNA methylation is extensively reconfigured over the course of mammalian development. While somatic tissue genomes remain hypermethylated following gastrulation, demethylation of specific genomic regions continues to occur during embryonic development (*9*, *13*). This developmental demethylation is believed to serve as a key epigenetic modality for lineage commitment, but its biologically critical functions in reshaping the chromatin state of a cell and its contribution to gene regulation and cell fate determination are less defined. In this study, we have provided six lines of evidence in support of a critical role for TET-dependent developmental DNA demethylation during specification of NSCs for establishing NSC identity and gliogenic competence: (i) NSCs established in the absence of TETs had limited self-renewal and selective impairment in forming glial cell types. (ii) TET deficiency prevented induction of neural- and glial-specific TFs in NSCs and during differentiation of NSCs to astrocytes and oligodendrocytes. (iii) Most regions that normally undergo developmental demethylation during NSC specification remained hypermethylated in the absence of TETs, and many were located at enhancers associated to down-regulated neural and glial genes in TKO NSCs. (iv) Hypermethylated neural and glial enhancers in TKO NSCs had reduced levels of H3K4me1 and H3K27ac, suggestive of impaired establishment and activation. (v) TET demethylase activity was sufficient to restore gene expression, self-renewal, and gliogenic competence of TKO NSCs. (vi) Deficiency of TETs in NSCs during mouse embryogenesis compromised glial gene expression and neuroanatomic development. These findings implicate TET-dependent developmental demethylation in commissioning neural and glial enhancers to activate neural programs and confer proper identity and gliogenic competence to NSCs (Fig. 9).

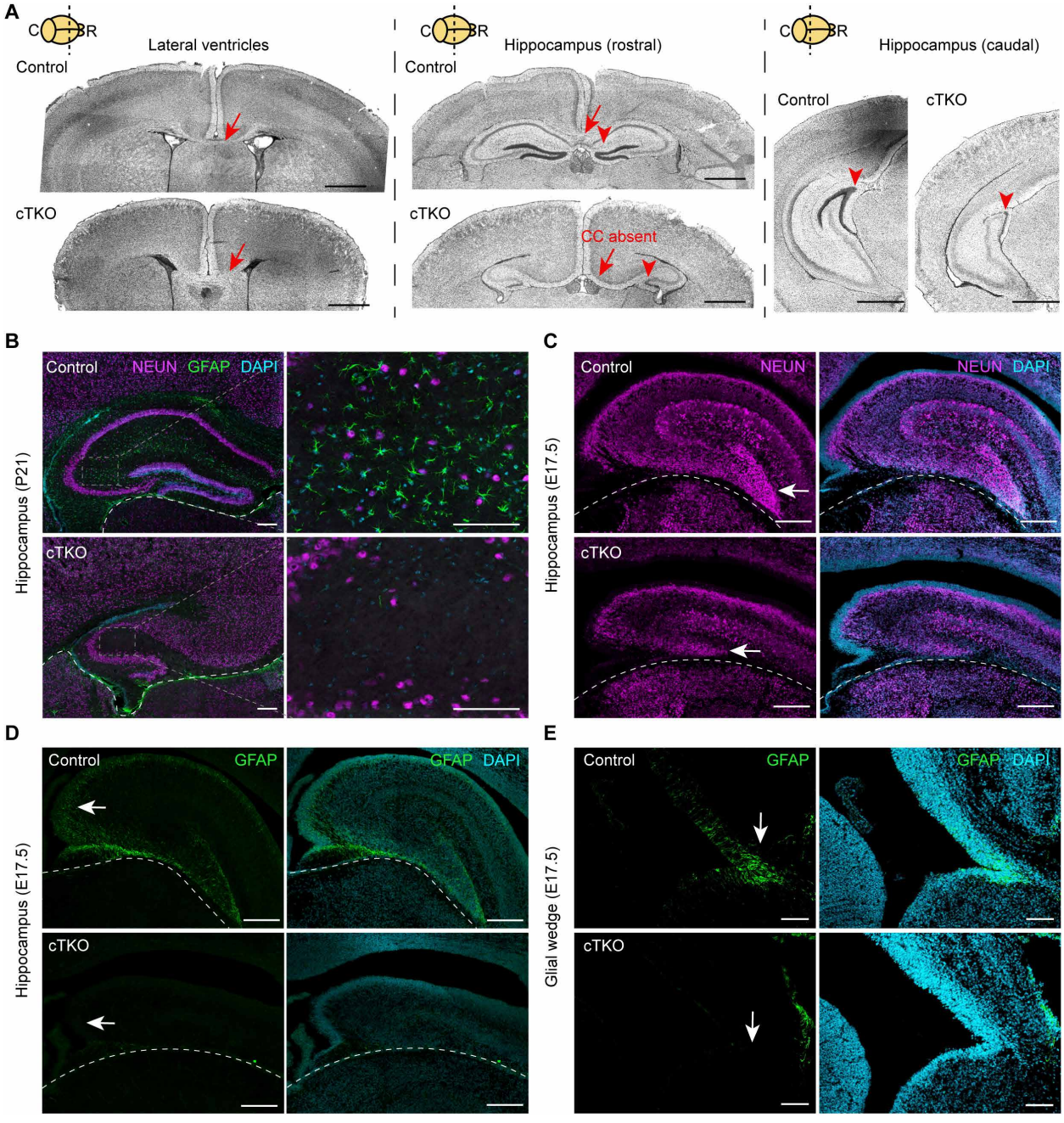

Fig. 8. Loss of TET enzymes in dorsal telencephalic NSCs compromises glial gene expression and corticogenesis. (**A**) Control and cTKO brain sections at the level of the lateral ventricles (left), rostral hippocampus (middle), and caudal hippocampus (right) stained with DAPI on P21. The dashed line in the cartoon indicates the approximate position of each section along the rostro (R)–caudal (C) axis. Arrows indicate the position of the corpus callosum. Arrowheads indicate the position of the dentate gyrus. Scale bars, 1 mm. (**B**) Control and cTKO P21 hippocampi stained for neuronal marker NEUN, astroglial marker GFAP, and DAPI. The left panels for each condition are at low magnification. Scale bars, 200 μm. Insets are shown at higher magnification in the right panels. Scale bars, 100 μm. (**C**) Control and cTKO E17.5 hippocampi stained for neuronal marker NEUN and DAPI. Arrows indicate dentate gyrus. Scale bars, 200 μm. (**D**) Control and cTKO E17.5 hippocampi stained for astroglial marker GFAP and DAPI. Arrows indicate the hippocampal ventricular zone. Scale bars, 200 μm. (**E**) Control and cTKO E17.5 cortices stained for astroglial marker GFAP and DAPI. Arrows indicate the glial wedge. Scale bars, 100 μm. Images representative of up to three biological replicates per group. For (B) to (E), areas above the white dashed lines are within the territory of *Emx1*^{Cre} expression.

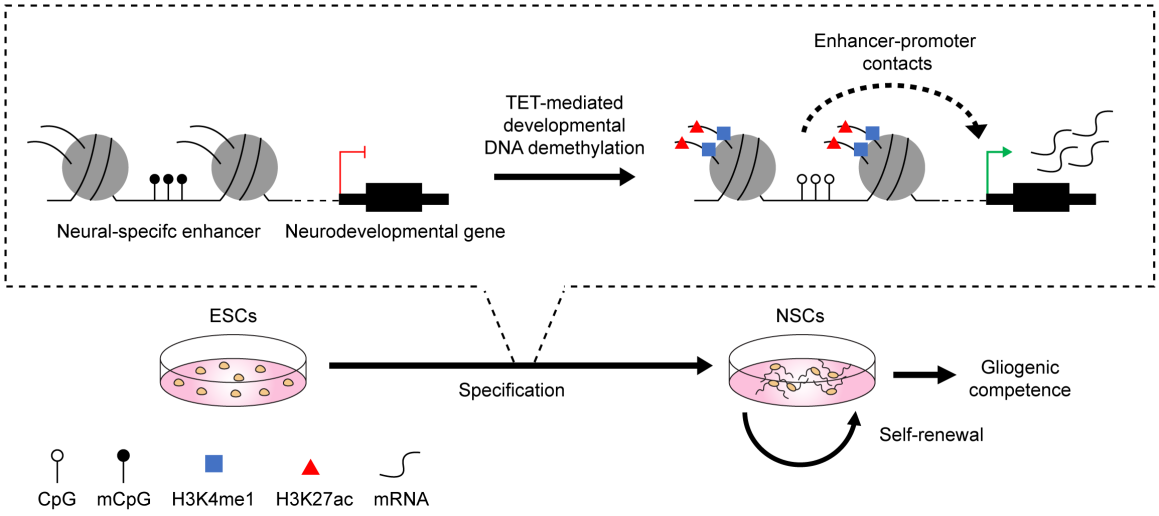

Fig. 9. TET-mediated developmental DNA demethylation commissions neural enhancers and confers NSC identity and gliogenic competence. TET-mediated DNA demethylation facilitates the commissioning of neural-specific enhancer elements and their contacts with target genes to promote expression of neurodevelopmental genes during NSC specification and confer acquisition of NSC identity, self-renewal, and gliogenic competence.

Developmental DNA demethylation has been observed in mammalian brains both during early organogenesis and late embryonic development (*9*, *13*). These postgastrulation demethylation events may be of particular importance for establishment of neural cell types arising during late gestation and early postnatal life, although functional studies involving ablation of the demethylation machinery in these contexts are lacking. Neural lineage specification is an ideal process for studying the functional significance of developmental DNA demethylation, as all three TET enzymes are dynamically expressed in the developing nervous system (*3*, *12*). Our utilization of a well-defined ESC-to-NSC differentiation platform has allowed us to test the requirement of TET-dependent demethylation in neural lineage commitment. Our findings that NESTIN-, SOX2-, and SOX1-expressing NSCs can be derived from TKO ESCs suggest that loss of TETs does not categorically block neural lineage commitment. However, the reduced expression of neural TFs by TET-deficient NSCs and their limited self-renewal and selective inability to form glial cell types are all indicative of compromised NSC identity. This, together with the fact that these phenotypes were rescued by TET demethylase activity, reveals a requirement for TET-dependent developmental demethylation during NSC specification to establish NSC identity and multipotency. The severe phenotypes of TKO NSCs contrast with the previously reported normal derivation of *Tet1* knockout NSCs and the mild apoptosis defect of *Tet3* knockout NSCs (*15*, *44*), supporting a high degree of redundancy among TETs in NSCs formation.

Our findings that TET enzymes are essential for demethylation of 76% (3294 of 4332) of regions that undergo developmental demethylation during NSC specification define TET enzymes as major epigenetic players in neural lineage commitment. The other 24% that do not require TETs likely constitute regions that are demethylated passively. Of the 3294 regions that were developmentally demethylated by TETs, 804 were located within 784 neural enhancers. These 784 enhancers constituted 18% of all neural-specific enhancers in NSCs and were the central focus of our work because many were associated with important neural and glial TF genes critical for NSC identity and multipotency. Although DNA demethylation at enhancers has long been observed, a general requirement for developmental DNA demethylation to ensure enhancer commissioning and interaction with target gene promoters has not been well established. Our findings that loss of TETs led to enhancer hypermethylation, prevented the deposition of H3K4me1 (the enhancer-commissioning mark) and H3K27ac (the enhancer activation mark), and reconfigured enhancer-promoter interactions suggest that TET-dependent enhancer demethylation during NSC specification is critical for enhancer commissioning and wiring of enhancer-promoter contacts. Previous studies have described TET occupancy, hydroxymethylation, and demethylation of lineage-specific enhancers in various contexts, for example, in embryonic (*23*, *45*), hematopoietic (*45*), and epidermal stem cells (*46*) and in vertebrate embryos (*9*). While studies have been informative regarding how loss of TET enzymes negatively affects enhancer activation, they have not defined a requirement for TETs in developmental enhancer commissioning (indicated by de novo deposition of H3K4me1) and establishment of enhancer-promoter contacts—roles we find to be essential for establishment of neural-specific gene expression during NSC specification. Our study takes a further critical step by linking the loss of enhancer commissioning and looping at these genes with functional deficits in NSC differentiation potential. Failure to demethylate and commission enhancers in proximity to glial TF genes of the *Nfi* and *Olig* families, major drivers of astrocyte and oligodendrocyte formation, respectively, correlated with their reduced expression and with a block in NSC differentiation into astrocytes and oligodendrocytes. Thus, one of the biologically critical functions of TET-dependent developmental DNA demethylation during NSC specification is to facilitate neural and glial enhancer commissioning to confer NSCs with proper identity and gliogenic competence.

The H3K4me1 methyltransferase mixed-lineage leukemia 4 (MLL4) is required both for commissioning and subsequent activation of enhancers (*40*, *47*). It is thus tempting to speculate that failure to recruit MLL4 due to hypermethylation might underlie the commissioning defect we observed. For example, in the context of adipocyte formation,

adipocyte pioneer factor C/EBPβ (a transcription factor, CCAAT/enhancer binding protein β) recruits MLL4 to commission adipocyte enhancers, and MLL4 binding is required for subsequent p300 recruitment and H3K27ac deposition (*40*, *47*). In the context of NSC specification, it is possible that TET-mediated enhancer demethylation is necessary for direct recruitment of MLL4 to enhancers or for binding of neural lineage TFs that facilitate MLL4 recruitment. Our findings that TET-regulated developmental DMRs were enriched for motifs of several SOX family TFs support such a model. A recent study reports a novel interaction between TET3 and MLL4 and their colocalization at active enhancers (*48*), further strengthening the connection between TET enzymes and enhancer-commissioning machinery. Follow-up work to map the occupancy of neural and glial lineage TFs and MLL4 in TET-deficient NSCs will shed further light on the relationship between developmental demethylation of enhancers and recruitment of lineage-specific TFs and chromatin modifiers.

During mouse development, NSC specification is coincident with gastrulation, and subsequent differentiation of NSCs during corticogenesis proceeds through two phases: first, a neurogenic phase from mid to late gestation during which NSCs exclusively produce neurons, followed by a gliogenic phase from late gestation to after birth during which NSCs produce glial cells (*49*). While investigations into the mechanisms underlying the developmental acquisition of gliogenic potential by NSCs have revealed numerous cell-extrinsic ligands and signaling molecules required for gliogenic competence (*49*), the required cell-intrinsic factors are less defined. DNA methylation is one intrinsic factor regulating gliogenesis, as loss of the maintenance DNA methyltransferase DNMT1 and the de novo methyltransferase DNMT3A in NSCs causes precocious astrocyte production (*50*, *51*). Here, we find that TET-dependent developmental demethylation is another intrinsic factor required for glial gene expression and NSC gliogenic competence. TET-dependent demethylation occurs in the vicinity of *Nfia/b/x* and *Olig1/2* and likely underpins the proper induction of these genes to promote astrocyte and oligodendrocyte formation (*29*, *31*–*33*, *52*). Our work expands on a recent study describing DNA demethylation events that occur in NSCs during acquisition of glial competence by demonstrating that a subset of this demethylation is TET dependent (*53*). We have further shown that loss of TET enzymes during mouse corticogenesis, similar to what occurs during NSC specification, compromised glial gene expression, as TET-deficient hippocampi lost GFAP expression and myelin component MBP was reduced in cortices. The neuroanatomic defects we observed in TET-deficient brains—partial corpus callosal agenesis and dentate gyrus hypoplasia—resemble those seen in mouse models of perturbed gliogenesis (*29*, *30*), raising the possibility that impaired glial gene expression may contribute to the observed defects. The period during which cTKO mice became runted (postnatal weeks 1 to 3) corresponds to the most robust wave of rodent cortical gliogenesis (*54*), further supporting a role for glia in the observed phenotypes.

We note that while our *Tet* TKO ESC-derived NSCs were unable to give rise to either astrocytes or oligodendrocytes based on expression of multiple marker genes, the dorsal telencephalic NSCs of cTKO mice could still form these cell types, as astrocyte-associated AQP4 and oligodendrocyte-associated OLIG2 were detected in cTKO brains. This discrepancy may be due to stage-specific requirements for TET enzymes in establishing varying degrees of gliogenic potential, as our TKO NSCs had been TET-deficient from the ESC stage, whereas cTKO NSCs lost TETs after NSC specification. Nevertheless, astroglial and oligodendrocytic gene expression were still compromised in cTKO brains, demonstrating that TETs are required for proper expression of glial programs even after NSCs have been specified. Our finding that acquisition of NSC gliogenic competence relies on TET enzymes is also consistent with reports describing a mild astrocytic differentiation defect upon *Tet2* knockdown in NSCs and subtle myelination defects upon conditional loss of TET1 in oligodendrocyte progenitors (*51*, *55*). However, the phenotypes observed in these and other studies of individual *Tet* knockout in the nervous system are not as severe as those we observed in TKO NSCs and cTKO mice (*11*), suggesting a high degree of redundancy among TETs in regulating neurodevelopment. While this work defines the requirement of TETs for acquisition of glial competence during formation of NSCs in vitro and in NSCs during embryogenesis, future work focused on tissue-specific deletion of TETs in astrocytes or oligodendrocytes may define unique roles of TETs after establishment of these cell types. This will also inform and dissect the developmental requirements of TETs in the genesis of glial cells versus the functional requirements of TETs in the biology of these cells. In addition, while TKO NSCs retained competence for neuronal differentiation, they produced neurons less efficiently than WT NSCs. Consistently, several of the deregulated, developmentally demethylated enhancers were associated with genes that are important for neurogenesis, such as *Rfx4* and *Pou3f3* (*56*, *57*). Therefore, it is likely that enhancer-commissioning defects that occur in the absence of TET-mediated demethylation negatively affect the neuronal differentiation capacity of TKO NSCs. This may also influence the functional properties of the neurons produced, as has been previously reported in the context of *Tet* TKO Purkinje neurons (*58*).

In summary, this study defines TET-dependent developmental DNA demethylation as a determinant of lineage-specific enhancer commissioning for proper specification of NSCs and acquisition of gliogenic competence. While this work primarily establishes the role of TET-dependent DNA demethylation in the specification of NSCs, it raises several interesting questions to be investigated in the future. First, while we have studied the effects of loss of all TETs during NSC establishment in vitro and in embryonic NSCs in vivo, the effects of TET loss in adult NSCs have been limited to single germline or conditional knockout mice, which exhibit mild learning and memory deficits (*11*). Future work studying loss of all three TETs in adult NSCs and mature neural cell types will define whether the roles of TETs in these contexts have parallels to those we have identified during NSC formation and in embryonic NSCs. Second, it will be interesting to explore the effects TET loss on specification of neuronal identity and function, particularly in the context of our $Emx1^{Cre}$ conditional *Tet* TKO mice, where it is possible that neuronal subtype proportions, lamination, or electrophysiology are affected. For example, conditional deletion of all TETs in postmitotic Purkinje neurons of the cerebellum causes sensitivity to excitotoxic drugs (*58*). Last, the paradigm of TET-dependent developmental demethylation for enhancer commissioning is possibly relevant to specification of other cell lineages beyond the nervous system, such as in the hematopoietic lineage where TETs are essential for embryonic hematopoiesis (*59*). Future work investigating DNA methylation dynamics during specification of other lineages will further broaden our understanding of developmental DNA demethylation in regulation of embryogenesis.

Limitations of the study

Our in vitro specification of NSCs from *Tet* TKO ESCs has enabled us to study the impact of loss of all three TETs on NSC formation and

biology. However, the early embryonic lethality of *Tet* TKO mice at gastrulation, the period during which neural induction occurs, limits our ability to study the effects of TET1/2/3 loss on NSC specification and gliogenic potential in vivo. A limitation of the $Emx1^{Cre}$ model is that it deletes *Tet1/2/3* after gastrulation and neural induction and consequently cannot be used to study NSC specification but rather NSC maintenance and multipotency. This likely underlies the difference in phenotypic severity between the in vitro derived TKO NSCs and the in vivo $Emx1^{Cre}$-recombined NSCs and may reflect stage-specific dependencies for TET enzymes in defining NSC identity, self-renewal, and multipotency. Moreover, the poor performance and reproducibility of existing commercial antibodies against each of the three TETs in high-throughput genomic occupancy applications such as ChIP-seq and CUT&RUN or CUT&Tag have limited our ability to map the occupancy of all TET enzymes with respect to enhancers and neural genes. These experiments would have been informative regarding the ability of TET enzymes to function redundantly at neural regulatory regions.

MATERIALS AND METHODS

Generation of *Tet1/2/3* TKO mouse ESCs

Tet1/2/3 TKO mouse ESCs (line v6.5, male, 129/B6 mixed background) were generated by CRISPR-Cas9 targeting of *Tet3* exon 4 in our published *Tet1/2* double knockout ESCs using our published protocols (*60*, *61*). Briefly, two pX330 plasmids expressing Cas9 and guide RNAs flanking *Tet3* exon 4 were transfected into *Tet1/2* double knockout ESCs to delete exon 4, resulting in an out-of-frame transcript and stop codon. Targeted clones were screened by PCR using previously published primers flanking exon 4 (*62*). Two independent TKO clones and three independent parental WT clones were validated and used for experiments.

Mouse ESC culture

ESCs were cultured on irradiated feeders in Dulbecco's modified Eagle's medium (DMEM) (Corning, 10-013-CV) with 10% fetal bovine serum (FBS) (Corning, 35-016-CV), 2 mM L-glutamine (Gibco, A29168-01), 1× nonessential amino acids (Gibco, 11140-050), penicillin (100 U/ml) with streptomycin (100 g/ml) (Gibco, 15140-122), leukemia inhibitory factor (LIF; 0.02 μg/ml), and 50 mM β-mercaptoethanol. For all experiments, ESCs were dissociated with TrypLE (Gibco, 12605-028) and preplated on 0.2% gelatin for 45 min to remove feeders before proceeding with downstream procedures.

Differentiation of ESC to NSCs

Differentiation of ESCs to NSCs was performed using the method of Okabe *et al.* (*24*) as modified in Lee *et al.* (*25*). Briefly, following preplating to remove feeders, 3 million to 5 million ESCs were seeded in 10-cm nonadherent petri dishes in the absence of LIF to form EBs over 4 days. EBs on day 4 were split 1:10, seeded onto tissue culture–treated 10-cm dishes, and allowed to adhere for 24 hours. Medium was then changed to ITSFn medium [DMEM/F-12 (Gibco, 11320-033] with insulin (5 μg/ml; Sigma-Aldrich, I6634), apotransferrin (50 μg/ml; Sigma-Aldrich, T2036), 30 nM sodium selenite (Sigma-Aldrich, S5261), fibronectin (5 μg/ml; Sigma-Aldrich, F4759), and penicillin (100 U/ml) with streptomycin (100 g/ml) (Gibco, 15140-122)]. Adherent EBs were cultured in ITSFn medium for 8 days to facilitate the outgrowth of NSCs after which cells were dissociated with Accutase (STEMCELL Technologies, 07922) and seeded onto poly-L-ornithine hydrobromide (Sigma-Aldrich, P3655) and laminin (Gibco, 23017015)–coated 6- or 12-well plates at a density of 1.0×10^5 to 1.5×10^5 cells/cm^2. NSCs were grown for 2 to 3 days before passage and downstream experiments.

NSC culture

Plates for NSC culture were coated first with poly-L-ornithine hydrobromide (15 μg/ml) overnight at 37°C and then with laminin (1 μg/ml) overnight at 37°C before seeding NSCs. NSCs were cultured in N2 medium [DMEM/F-12 with insulin (25 μg/ml), apotransferrin (50 μg/ml), 20 nM progesterone (Sigma-Aldrich, P8783), 100 μM putrescine (Sigma-Aldrich, P5780), 30 nM sodium selenite, penicillin (100 U/ml), and streptomycin (100 g/ml)] supplemented with epidermal growth factor (20 ng/ml; R&D Systems, 236-EG), basic fibroblast growth factor (bFGF) (10 ng/ml; R&D Systems, 233-FB), and laminin (1 μg/ml). For routine passage, NSCs were seeded at a density of 1.0×10^5 to 1.5×10^5 cells/cm^2 and passaged every 2 to 3 days after dissociation with Accutase. For quantitative assessment of growth, cells of each genotype were seeded at 1.5×10^5 cells/cm^2 or at the maximum density possible if fewer cells were obtained and passaged every 2 to 3 days. Cumulative cell number was calculated by multiplying the cell counts at each passage by the product of the reciprocal fractions of cells seeded at prior passages. Cells were counted with a hemocytometer, and cell viability was determined using trypan blue exclusion. For all immunofluorescence, multipotency, transcriptomic, and epigenomic experiments, NSCs were harvested or analyzed after one passage (between 4 and 6 days of NSC culture).

NSC differentiation to neurons, astrocytes, and oligodendrocytes

For all lineage-specific differentiations, NSCs at passage one (day 6) were seeded into Matrigel growth factor reduced (Corning, 354230)–coated wells. For wells used for immunofluorescence staining, coverslips were placed in wells before coating. (i) Neuron differentiation was adapted from the protocol of Gouti *et al.* (*63*) as follows: NSCs were seeded at a density of 1.0×10^5 cells/cm^2 in N2/B27 medium [1:1 ratio of N2 medium to neurobasal medium (Gibco, 21103-049) with B27 supplement (Gibco, 17504-044), 2 mM L-glutamine, penicillin (100 U/ml), and streptomycin (100 g/ml)] with bFGF (10 ng/ml) and cultured for 24 hours. Medium was then changed to N2/B27 medium with no growth factors, and cells were cultured for a further 72 hours. (ii) Astrocyte differentiation was adapted from the protocol of Belenguer *et al.* (*64*) as follows: NSCs were seeded at a density of 1.0×10^5 cells/cm^2 in N2 medium with bFGF (10 ng/ml) and cultured for 24 hours. Medium was then changed to N2 medium with 2% FBS, and cells were cultured for a further 72 hours. (iii) For oligodendrocyte differentiation, NSCs were seeded at a density of 1.0×10^5 cells/cm^2 in N2/B27 medium with bFGF (10 ng/ml) and cultured for 24 hours. Medium was then changed to N2/B27 medium with triiodo-L-thyronine (30 ng/ml; Sigma-Aldrich, T5516) and cultured for a further 72 hours. For all three differentiations, at 96 hours, cells in wells for RNA extraction were lysed directly in wells, and RNA was isolated using the Omega EZNA Total RNA Kit according to the manufacturer's instructions. Cells in wells for immunofluorescence staining were fixed, and immunofluorescence was carried out as described below.

Immunofluorescence staining

Immunofluorescence staining of NSCs and differentiated neural cells was adapted from the protocol of Belenguer *et al.* (*64*). For immunofluorescence of NSCs, cells were cultured on Matrigel growth

factor reduced–coated coverslips for 24 hours before fixation. Cells were fixed with 2% paraformaldehyde (Thermo Fisher Scientific, 043368.9M) for 15 min at 37°C and then blocked in Dulbecco's phosphate-buffered saline (DPBS) (Corning, 21-031-CV) with 10% FBS and 1% glycine for 1 hour at room temperature. Primary antibodies {anti-NESTIN (1:200; Millipore, MAB353), anti-SOX2 (1:200; Millipore, AB5603), anti-SOX1 [1:200; Cell Signaling Technology (CST), 4194], anti-TUJ1 (1:150; CST, 5568), anti-GFAP (1:300; CST, 3670), and anti-O4 (5 μg/ml; R&D Systems, MAB1326)} were incubated overnight at 4°C in DPBS with 0.1% Triton X-100 (Fisher, BP151-100), 10% FBS, and 1% glycine (Sigma-Aldrich). Secondary antibodies [anti-mouse Alexa Fluor 488 (1:500; Invitrogen, A32766), anti-mouse Alexa Fluor 594 (1:500; Invitrogen, A-21207), anti-rabbit Alexa Fluor 594 (1:500; Invitrogen, A-11012), and anti-goat Alexa Fluor 488 (1:500; Invitrogen, A32814)] were incubated at room temperature for 1 hour in DPBS with 0.1% Triton X-100, 10% FBS, and 1% glycine. Cells were stained with 4′,6-diamidino-2-phenylindole (DAPI) (5 ng/ml in DPBS) for 1 min. Coverslips were mounted with VECTASHIELD Antifade Mounting Medium (VectorLabs, H-1000) onto Superfrost Plus slides (Fisher, 12-550-15) and imaged with a Zeiss Apotome.2 fluorescence microscope. For anti-O4 antibody staining, Triton X-100 was omitted from all steps.

Reverse transcription quantitative polymerase chain reaction

RT-qPCR was performed as previously described (*26*). Briefly, RNA was extracted using the Omega EZNA Total RNA Kit (R6834-02) following the manufacturer's protocols. cDNA was synthesized using the SuperScript III kit (Invitrogen, 18080-400) according to the manufacturer's instructions. Ten nanograms of cDNA per reaction was used for RT-qPCR with Fast SYBR Green Master Mix (Thermo Fisher Scientific, 4385612) and primers (table S1) (*15*, *22*, *26*, *32*, *60*, *62*, *65*–*68*) on a BD Applied Biosystems StepOne Real-Time PCR System.

RNA-seq and data analysis

RNA-seq was performed as previously described (*26*). Three WT and two TKO ESC and NSC biological replicates were used. ESCs were preplated to remove feeder cells and then harvested. NSCs were harvested at passage one (day 6) of culture. RNA was extracted with the Omega EZNA Total RNA Kit I. Library preparation and 150–base pair (bp) paired-end sequencing were performed at Novogene. Libraries were sequenced using the Illumina NovoSeq 6000 platform. Adaptor and low-quality trimming were performed with trim galore (v0.6.5, www.bioinformatics.babraham.ac.uk/projects/trim_galore/). Clean reads were mapped to *Mus musculus* reference genome mm10 using STAR (v2.7.3a) (*69*) with default parameters. Counts were extracted from mapped reads with featureCounts using the –largestOverlap parameter. DESeq2 (v1.40.2) (*70*) was used to identify DEGs (FDR < 0.05, fold change > 2) from raw counts using the standard package documentation. Gene ontology terms were identified on selected sets of DEGs using DAVID (*71*). Statistical significance of gene set enrichments was performed using the hypergeometric test.

WGBS and data analysis

ESCs were preplated to remove feeder cells and then grown in gelatin-coated wells for 24 hours before harvest. NSCs were harvested at passage one (day 6) of culture. One WT and one TKO replicates were processed per cell type. DNA was extracted with the Quick-DNA Miniprep Kit (Zymo, D3024) according to the manufacturer's instructions. Bisulfite conversion, library preparation, and 100-bp paired-end sequencing on a DNA nanoball sequencing platform were performed at BGI Genomics. Raw read filtering was performed by BGI Genomics using SOAPnuke (*72*) with the parameters -n 0.001 -l 20 -q 0.4 –adaMR 0.25 –ada_trim –polyX 50 to remove adaptors and filter out low-quality reads. Clean reads were mapped to mm10 using Bismark (v0.22.3) (*73*) with default parameters. Read deduplication was performed using deduplicate_bismark, and cytosine methylation levels were extracted with bismark_methylation_extractor. BAM files were balanced to the sample with the lowest number of reads with SAMtools (v1.9) (*74*). DMRs were identified between TKO ESC versus WT ESC, TKO NSC versus WT NSC, and WT NSC versus WT ESC using MethPipe (v3.4.3) (*75*) with standard parameters (regions with >5 CpGs, methylation different > 20%, and FDR < 0.05). Bedtools2 (v 2.28.0) (*76*) was used to define NSC TKO devDMRs and non-devDMRs as follows: First, any NSC TKO hyperDMR with a minimum 1 bp overlap with an ESC TKO hyperDMR was excluded using the intersect function with option -v. NSC TKO devDMRs were defined by intersecting the resulting NSC-unique TKO hyperDMRs with developmental hypoDMRs using the intersect function with option -u. NSC TKO non-devDMRs were defined by intersecting NSC-unique TKO hyperDMRs with developmental hypoDMRs using the intersect function with option -v. DMRs were annotated to genomic regions with the R package ChIPseeker (v1.30.3) (*77*). Promoter regions were defined as ±2 kb of TSS. DMRs were assigned to genes based on the closest TSS. Motif analysis of DMRs was performed with HOMER (v4.7) (*78*), and its known motifs output was reported. SOX2, SOX3, and SOX9 ChIP-seq peaks were downloaded in BED format as reported by Bergsland *et al.* (*35*) and Klum *et al.* (*36*). Peaks in mm9 coordinates were converted to mm10 using the UCSC LiftOver tool (https://genome.ucsc.edu/cgi-bin/hgLiftOver). NSC TKO devDMRs were intersected with ChIP-seq peaks using bedtools intersect with option -u. The 60-way vertebrate phastCons score BigWig file for mm10 was downloaded from UCSC Genome Browser (http://hgdownload.cse.ucsc.edu/goldenpath/mm10/phastCons60way/) (*79*). E11.5 mouse WGBS data were downloaded in BED format from the ENCODE Project Consortium (*37*). BED files were converted to bedGraph format and then converted to BigWig format using the command bedGraphToBigWig (*80*). E11.5 mouse H3K27ac ChIP-seq data were downloaded from ENCODE in BigWig format and plotted without further processing. See table S2 for a complete list of ENCODE WGBS and ChIP-seq accession numbers. Profile plots of WGBS, phastCons, and ChIP-seq data were generated from BigWig files using DeepTools (v4.5.1) (*81*). Genome browser tracks were generated using pyGenomeTracks (*82*). Integration of NSC TKO devDMRs with validated enhancers from the VISTA Enhancer Browser database (Lawrence Berkeley National Laboratory, https://enhancer.lbl.gov/) (*38*) was performed as follows: BED files of highly conserved elements with validated enhancer activity were downloaded from the VISTA Enhancer Browser database in mm9 coordinates. Enhancer coordinates were converted from mm9 to mm10 using the UCSC LiftOver tool. Enhancers were intersected with NSC TKO devDMRs using bedtools intersect with option -u. Enhancers were classified as having neural activity if reproducible LacZ staining was observed in the forebrain, midbrain, hindbrain, neural tube, cranial nerve, trigeminal V, eye, or dorsal root ganglion.

CUT&Tag and data analysis

Genome-wide mapping of H3K4me1 and H3K27ac was performed by CUT&Tag as previously described (*26*, *83*). Two biological replicates

per genotype and cell type were analyzed. ESCs were preplated to remove feeder cells and then grown in gelatin-coated wells for 24 hours before harvest. NSCs were harvested at passage one (day 6) of culture. A total of 1.0×10^5 cells per genotype and condition were washed in DPBS and cross-linked with 0.5% paraformaldehyde for 5 min. Cross-linking was quenched by addition of glycine to 375 mM. Cells were bound to concanavalin A–coated beads (Epicypher, 21-1401), permeabilized, and incubated with 1 μg of primary antibody [anti-H3K4me1 (Abcam, ab8895), anti-H3K27ac (Abcam, ab4729), and rabbit immunoglobulin G (IgG) isotype control (CST, 3900)] overnight at 4°C. Samples were incubated with secondary antibody (guinea pig anti-rabbit, Antibodies Online, ABIN101961) for 1 hour at room temperature. Preloaded pA-Tn5 transposase-adaptor complex (a gift from A. Skoultchi, Albert Einstein College of Medicine) was then added, and samples were incubated for 1 hour at room temperature. Transposase was activated by incubation in tagmentation buffer with magnesium for 1 hour at 37°C. Adaptor-ligated DNA was isolated by phenol-chloroform isoamyl alcohol extraction and amplified using NEBNext High Fidelity 2× PCR Master Mix (M0541). Post-PCR DNA libraries were cleaned up with AMPure XP beads (Beckman Coulter, A63880). Libraries were subjected to 75-bp paired-end sequencing on the Illumina NextSeq 500 platform at the Einstein Epigenomics Shared Facility. Adaptor and low-quality trimming were performed with trim galore. Clean reads were mapped to mm10 using bowtie2 (*84*) using options -local -sensitive -very-sensitive-local --no-unal -no-mixed -no-discordant -phred33 -I 10 -X 700. Duplicate reads were removed with Picard tools (v2.26.10, https://broadinstitute.github.io/picard/). Peak calling was performed first before data balancing with SEACR (v1.3) (*85*) using options -norm and -stringent and with the IgG control for each cell type as background. The fraction of reads in peaks (FRiP) was calculated from the SEACR output BED file and the unbalanced BAM files. BAM files were then balanced across all samples for each histone mark to the sample with the lowest number of reads in peaks (product of the FRiP and the number of reads). Peaks were then called again with SEACR using the balanced BAM files to obtain the final peak sets. DeepTools was used to convert balanced BAM files to BigWig files using the bamCoverage function with parameter -binsize 10 and to generate profile plots and heatmaps. Genome browser tracks were generated using pyGenomeTracks.

Identification of NSC-unique active enhancers and differential H3K4me1 and H3K27ac analysis

First, consensus peaks between biological replicates for all samples were defined using bedtools intersect with default settings to find the intersection of the individual peak BED files. Then, for each cell type and genotype, H3K4me1 and H3K27ac double positive peaks were defined with bedtools intersect using the consensus H3K4me1 and H3K27ac BED files. Next, for each genotype, ESC double positive peaks were excluded using bedtools intersect with option -v to obtain NSC-unique double positive peaks. NSC-unique double positive peaks were annotated to genomic regions using ChIPseeker. Last, peaks annotated to promoter regions (±2 kb of TSS) were excluded to obtain WT and TKO NSC-unique active enhancers. Enhancers were assigned to genes based on their proximity to the nearest TSS. H3K4me1 and H3K27ac levels at NSC-unique active enhancers were quantified using DiffBind (v3.10.0) (*86*). First, WT and TKO NSC-unique active enhancer BED files were merged using bedtools merge to obtain a master set of NSC-unique active enhancers. Then, DiffBind was run between TKO and WT NSC using the merged enhancer BED file and balanced H3K4me1 and H3K27ac BAM files as inputs. Differential enrichment of H3K4me1 and H3K27ac at enhancers was determined using a *P* value threshold of 0.05.

Promoter-capture HiC

Genomic regions interacting with gene promoters in WT and TKO NSCs were identified using promoter-capture HiC. A total of 10 million NSCs at passage one were harvested and cross-linked with 2% paraformaldehyde (PFA) for 10 min at room temperature. Cross-linking was quenched by addition of glycine to 230 μM. HiC library preparation, promoter capture, sequencing, and chromatin loop calling were performed by Arima Genomics. Each sample was sequenced to a depth of 170 million to 190 million raw read pairs. Data were processed using the Arima Capture-HiC v1.5 pipeline. Briefly, reads were aligned to mm10 using HiCUP, and chromatin loops were called at 5-kb resolution using CHiCAGO (*87*, *88*). To identify total differential loops between WT and TKO NSCs, the bedtools function pairToPair was used with option -notboth. To identify differential loops at active enhancers containing NSC TKO devDMRs, WT and TKO promoter-interacting loops were first overlapped with these enhancers using the bedtools function pairtobed with option -either. Then, the WT and TKO enhancer loops were compared using pairToPair with option -notboth. Genome browser tracks were generated using the Washington University Epigenome Browser.

Lentivirus preparation and transduction

Lentivirus was prepared as previously described (*89*). Briefly, FUW-tdTomato (empty) or FUW-expressing hemagglutinin (HA)–tagged *Tet1* WT or mutant catalytic domain and tdTomato (FUW-HA-TET1CD-2A-tdTomato or FUW-HA-TET1CD-2A-tdTomato) were transfected into human embryonic kidney–293T cells along with psPAX2 and pMD2.G using XtremeGene 9 DNA transfection reagent. Viral supernatants were concentrated with Lenti-X Concentrator (Takara, 631231). TKO ESCs were transduced for 48 hours, and tdTomato$^+$ cells were sorted by fluorescence activated cell sorting (FACS) 24 hours later and then cultured on feeders. After ~1 week in culture, individual tdTomato$^+$ ESC colonies with comparable expression of tdTomato were picked and pooled to obtain populations with homogenous tdTomato expression.

Generation of *Tet* cTKO mice

B6.129S2-*Emx1*$^{tm1(cre)Krj}$/J (*Emx*$^{Cre/Cre}$) mice were obtained from the Jackson Laboratory (strain 005628) (*42*). Because of the very close genetic linkage between the *Emx1* and *Tet3* loci on chromosome 6 that prevented segregation of *Emx1*^{Cre} with a *Tet3*^{f} allele in our crosses, we disrupted the *Tet3* allele in *Emx1*$^{Cre/Cre}$ zygotes by CRISPR-Cas9. *Z*ygotes were injected with Cas9 protein and a previously published single guide RNA targeting the *Tet3* catalytic domain at the Einstein Transgenic Facility (*62*). Manipulated zygotes were implanted into pseudo-pregnant females, and offspring were screened by PCR for insertions or deletions within the *Tet3* catalytic domain. A heterozygous 60-bp deletion spanning the critical iron-binding site required for catalytic activity was identified in a founder male and confirmed by Sanger sequencing (*2*). This male was crossed to 129/B6 mixed background WT females. Homozygosity of this *Tet3* allele exhibited perinatal lethality, which is the expected phenotype of *Tet3*$^{-/-}$ mice (*18*). This confirmed the allele to be functionally null, and we therefore refer to it as *Tet3*$^{-}$. Next, male *Emx1*$^{+/Cre}$;*Tet3*$^{+/-}$ and female *Tet1*$^{f/f}$;*Tet2*$^{f/f}$ mice were mated to obtain *Emx1*$^{+/Cre}$;*Tet1*$^{+/f}$;*Tet2*$^{+/f}$;*Tet3*$^{+/-}$ mice.

Last, 2- to 3-month-old male *Emx1*$^{+/Cre}$;*Tet1*$^{+/f}$;*Tet2*$^{+/f}$;*Tet3*$^{+/-}$ and female *Emx1*$^{+/+}$;*Tet1*$^{f/f}$;*Tet2*$^{f/f}$;*Tet3*$^{f/f}$ mice were mated to obtain experimental *Emx1*$^{+/Cre}$;*Tet1*$^{f/f}$;*Tet2*$^{f/f}$;*Tet3*$^{f/-}$ (*Tet* cTKO) embryos and mice. All experiments were performed in accordance with our approved Albert Einstein College of Medicine Institutional Animal Care and Use Committee protocols study approval number 00001310.

Mouse perfusion, brain cryosectioning, and immunofluorescence

For P21 brains, *Tet* cTKO and littermate control (*Emx1*$^{+/+}$) mice were perfused with DPBS, followed by 4% PFA. Brains were dissected, post-fixed overnight in 4% PFA at 4°C, and cryoprotected in a 15 to 30% sucrose gradient at 4°C. For embryonic E17.5 brains, time-mated dams were euthanized, and embryos were isolated. For immunofluorescence analysis, up to three biological replicates per group were analyzed. Brains were dissected, washed with DPBS, and fixed overnight in 4% PFA at 4°C before cryoprotection as above. Brains were embedded in O.C.T. compound (Sakura, 4583), and 20-µm sections were sliced on a Leica CryoStar NX50 cryostat. Sections were mounted onto Superfrost Plus slides, permeabilized in DPBS with 0.5% Triton X-100 for 10 min, and blocked in DPBS with 3% bovine serum albumin (BSA) and 0.1% Triton X-100 for 1 hour at room temperature. Primary antibodies [anti-GFAP (1:400; CST, 3670, for P21 brains), anti-GFAP (1:500; Dako, Z00334, for embryonic brains), anti-NEUN (1:100; CST, 24307), anti-SOX2 (1:200; Millipore, AB5603), anti-MBP (1:50; Abcam, ab7349), anti-OLIG2 (10 µg/ml; R&D Systems, AF2418), and anti-AQP4 (1:800; CST, 59678)] in DPBS with 3% BSA and 0.1% Triton X-100 were incubated overnight at 4°C. Secondary antibodies [anti-mouse Alexa Fluor 594 (1:500; Invitrogen, A-21207), anti-rabbit Alexa Fluor 488 (1:500; Invitrogen, A21206), and anti-rat Alexa Fluor 555 (1:500; Southern Biotech, 6430-32)] in DPBS with 3% BSA and 0.1% Triton X-100 were incubated at room temperature for 1 hour. Sections were stained with DAPI (5 ng/ml in DPBS) for 5 min. Coverslips were applied with ProLong Glass mounting medium (Invitrogen, P36980) and cured overnight at room temperature. Slides were imaged with a Zeiss Apotome.2 fluorescence microscope.

Statistical analysis

GraphPad Prism (v8.4.3), bedtools2 (v2.28.0), and R software (v4.0.3) were used for statistical analyses. Unpaired Student's *t* test was used to compare two groups. One-way analysis of variance (ANOVA) was used to compare more than two groups. Differences in proportions were assessed by two-proportion *z* tests. Enrichment and depletion of groups for features were assessed with the hypergeometric test. Significance of feature overlaps was determined by 10^3 random permutation tests. *P* values were adjusted for multiple testing correction where applicable. Statistical analyses for genome-wide methods are explained in detail under the respective methods subsections.

Supplementary Materials

The PDF file includes:

Figs. S1 to S7
Tables S1 and S2
Legend for data S1

Other Supplementary Material for this manuscript includes the following:

Data S1

REFERENCES AND NOTES

1. M. V. C. Greenberg, D. Bourc'his, The diverse roles of DNA methylation in mammalian development and disease. *Nat. Rev. Mol. Cell Biol.* **20**, 590–607 (2019).
2. M. Tahiliani, K. P. Koh, Y. Shen, W. A. Pastor, H. Bandukwala, Y. Brudno, S. Agarwal, L. M. Iyer, D. R. Liu, L. Aravind, A. Rao, Conversion of 5-methylcytosine to 5-hydroxymethylcytosine in mammalian DNA by MLL partner TET1. *Science* **324**, 930–935 (2009).
3. M. A. Hahn, R. Qiu, X. Wu, A. X. Li, H. Zhang, J. Wang, J. Jui, S. G. Jin, Y. Jiang, G. P. Pfeifer, Q. Lu, Dynamics of 5-hydroxymethylcytosine and chromatin marks in Mammalian neurogenesis. *Cell Rep.* **3**, 291–300 (2013).
4. M. Bachman, S. Uribe-Lewis, X. Yang, M. Williams, A. Murrell, S. Balasubramanian, 5-Hydroxymethylcytosine is a predominantly stable DNA modification. *Nat. Chem.* **6**, 1049–1055 (2014).
5. S. Ito, L. Shen, Q. Dai, S. C. Wu, L. B. Collins, J. A. Swenberg, C. He, Y. Zhang, Tet proteins can convert 5-methylcytosine to 5-formylcytosine and 5-carboxylcytosine. *Science* **333**, 1300–1303 (2011).
6. Y. F. He, B. Z. Li, Z. Li, P. Liu, Y. Wang, Q. Tang, J. Ding, Y. Jia, Z. Chen, L. Li, Y. Sun, X. Li, Q. Dai, C. X. Song, K. Zhang, C. He, G. L. Xu, Tet-mediated formation of 5-carboxylcytosine and its excision by TDG in mammalian DNA. *Science* **333**, 1303–1307 (2011).
7. F. Marlétaz, P. N. Firbas, I. Maeso, J. J. Tena, O. Bogdanovic, M. Perry, C. D. R. Wyatt, E. de la Calle-Mustienes, S. Bertrand, D. Burguera, R. D. Acemel, S. J. van Heeringen, S. Naranjo, C. Herrera-Ubeda, K. Skvortsova, S. Jimenez-Gancedo, D. Aldea, Y. Marquez, L. Buono, I. Kozmikova, J. Permanyer, A. Louis, B. Albuixech-Crespo, Y. Le Petillon, A. Leon, L. Subirana, P. J. Balwierz, P. E. Duckett, E. Farahani, J. M. Aury, S. Mangenot, P. Wincker, R. Albalat, È. Benito-Gutiérrez, C. Canestro, F. Castro, S. D'Aniello, D. E. K. Ferrier, S. Huang, V. Laudet, G. A. B. Marais, P. Pontarotti, M. Schubert, H. Seitz, I. Somorjai, T. Takahashi, O. Mirabeau, A. Xu, J. K. Yu, P. Carninci, J. R. Martinez-Morales, H. R. Crollius, Z. Kozmik, M. T. Weirauch, J. Garcia-Fernàndez, R. Lister, B. Lenhard, P. W. H. Holland, H. Escriva, J. L. Gómez-Skarmeta, M. Irimia, Amphioxus functional genomics and the origins of vertebrate gene regulation. *Nature* **564**, 64–70 (2018).
8. A. de Mendoza, R. Lister, O. Bogdanovic, Evolution of DNA methylome diversity in eukaryotes. *J. Mol. Biol.* **432**, 1687–1705 (2020).
9. O. Bogdanovic, A. H. Smits, E. de la Calle Mustienes, J. J. Tena, E. Ford, R. Williams, U. Senanayake, M. D. Schultz, S. Hontelez, I. van Kruijsbergen, T. Rayon, F. Gnerlich, T. Carell, G. J. Veenstra, M. Manzanares, T. Sauka-Spengler, J. R. Ecker, M. Vermeulen, J. L. Gomez-Skarmeta, R. Lister, Active DNA demethylation at enhancers during the vertebrate phylotypic period. *Nat. Genet.* **48**, 417–426 (2016).
10. S. Kriaucionis, N. Heintz, The nuclear DNA base 5-hydroxymethylcytosine is present in Purkinje neurons and the brain. *Science* **324**, 929–930 (2009).
11. I. C. MacArthur, M. M. Dawlaty, TET enzymes and 5-hydroxymethylcytosine in neural progenitor cell biology and neurodevelopment. *Front. Cell Dev. Biol.* **9**, 645335 (2021).
12. R. Khoueiry, A. Sohni, B. Thienpont, X. Luo, J. V. Velde, M. Bartoccetti, B. Boeckx, A. Zwijsen, A. Rao, D. Lambrechts, K. P. Koh, Lineage-specific functions of TET1 in the postimplantation mouse embryo. *Nat. Genet.* **49**, 1061–1072 (2017).
13. R. Lister, E. A. Mukamel, J. R. Nery, M. Urich, C. A. Puddifoot, N. D. Johnson, J. Lucero, Y. Huang, A. J. Dwork, M. D. Schultz, M. Yu, J. Tonti-Filippini, H. Heyn, S. Hu, J. C. Wu, A. Rao, M. Esteller, C. He, F. G. Haghighi, T. J. Sejnowski, M. M. Behrens, J. R. Ecker, Global epigenomic reconfiguration during mammalian brain development. *Science* **341**, 1237905 (2013).
14. A. Ruzov, Y. Tsenkina, A. Serio, T. Dudnakova, J. Fletcher, Y. Bai, T. Chebotareva, S. Pells, Z. Hannoun, G. Sullivan, S. Chandran, D. C. Hay, M. Bradley, I. Wilmut, P. De Sousa, Lineage-specific distribution of high levels of genomic. *Cell Res.* **21**, 1332–1342 (2011).
15. M. M. Dawlaty, K. Ganz, B. E. Powell, Y. C. Hu, S. Markoulaki, A. W. Cheng, Q. Gao, J. Kim, S. W. Choi, D. C. Page, R. Jaenisch, Tet1 is dispensable for maintaining pluripotency and its loss is compatible with embryonic and postnatal development. *Cell Stem Cell* **9**, 166–175 (2011).
16. Z. Li, X. Cai, C. L. Cai, J. Wang, W. Zhang, B. E. Petersen, F. C. Yang, M. Xu, Deletion of Tet2 in mice leads to dysregulated hematopoietic stem cells and subsequent development of myeloid malignancies. *Blood* **118**, 4509–4518 (2011).
17. A. Rudenko, M. M. Dawlaty, J. Seo, A. W. Cheng, J. Meng, T. Le, K. F. Faull, R. Jaenisch, L. H. Tsai, Tet1 is critical for neuronal activity-regulated gene expression and memory extinction. *Neuron* **79**, 1109–1122 (2013).
18. T. P. Gu, F. Guo, H. Yang, H. P. Wu, G. F. Xu, W. Liu, Z. G. Xie, L. Shi, X. He, S. G. Jin, K. Iqbal, Y. G. Shi, Z. Deng, P. E. Szabo, G. P. Pfeifer, J. Li, G. L. Xu, The role of Tet3 DNA dioxygenase in epigenetic reprogramming by oocytes. *Nature* **477**, 606–610 (2011).
19. H. Q. Dai, B. A. Wang, L. Yang, J. J. Chen, G. C. Zhu, M. L. Sun, H. Ge, R. Wang, D. L. Chapman, F. Tang, X. Sun, G. L. Xu, TET-mediated DNA demethylation controls gastrulation by regulating Lefty-Nodal signalling. *Nature* **538**, 528–532 (2016).
20. S. Cheng, M. Mittnenzweig, Y. Mayshar, A. Lifshitz, M. Dunjic, Y. Rais, R. Ben-Yair, S. Gehrs, E. Chomsky, Z. Mukamel, H. Rubinstein, K. Schlereth, N. Reines, A. H. Orenbuch, A. Tanay, Y. Stelzer, The intrinsic and extrinsic effects of TET proteins during gastrulation. *Cell* **185**, 3169–3185.e20 (2022).

21. S. J. Clark, R. Argelaguet, T. Lohoff, F. Krueger, D. Drage, B. Gottgens, J. C. Marioni, J. Nichols, W. Reik, Single-cell multi-omics profiling links dynamic DNA methylation to cell fate decisions during mouse early organogenesis. *Genome Biol.* **23**, 202 (2022).
22. M. M. Dawlaty, A. Breiling, T. Le, M. I. Barrasa, G. Raddatz, Q. Gao, B. E. Powell, A. W. Cheng, K. F. Faull, F. Lyko, R. Jaenisch, Loss of Tet enzymes compromises proper differentiation of embryonic stem cells. *Dev. Cell* **29**, 102–111 (2014).
23. F. Lu, Y. Liu, L. Jiang, S. Yamaguchi, Y. Zhang, Role of Tet proteins in enhancer activity and telomere elongation. *Genes Dev.* **28**, 2103–2119 (2014).
24. S. Okabe, K. Forsberg-Nilsson, A. C. Spiro, M. Segal, R. D. McKay, Development of neuronal precursor cells and functional postmitotic neurons from embryonic stem cells in vitro. *Mech. Dev.* **59**, 89–102 (1996).
25. S. H. Lee, N. Lumelsky, L. Studer, J. M. Auerbach, R. D. McKay, Efficient generation of midbrain and hindbrain neurons from mouse embryonic stem cells. *Nat. Biotechnol.* **18**, 675–679 (2000).
26. S. Chrysanthou, Q. Tang, J. Lee, S. J. Taylor, Y. Zhao, U. Steidl, D. Zheng, M. M. Dawlaty, The DNA dioxygenase Tet1 regulates H3K27 modification and embryonic stem cell biology independent of its catalytic activity. *Nucleic Acids Res.* **50**, 3169–3189 (2022).
27. B. Deneen, R. Ho, A. Lukaszewicz, C. J. Hochstim, R. M. Gronostajski, D. J. Anderson, The transcription factor NFIA controls the onset of gliogenesis in the developing spinal cord. *Neuron* **52**, 953–968 (2006).
28. J. Tchieu, E. L. Calder, S. R. Guttikonda, E. M. Gutzwiller, K. A. Aromolaran, J. A. Steinbeck, P. A. Goldstein, L. Studer, NFIA is a gliogenic switch enabling rapid derivation of functional human astrocytes from pluripotent stem cells. *Nat. Biotechnol.* **37**, 267–275 (2019).
29. T. Shu, K. G. Butz, C. Plachez, R. M. Gronostajski, L. J. Richards, Abnormal development of forebrain midline glia and commissural projections in *Nfia* knock-out mice. *J. Neurosci.* **23**, 203–212 (2003).
30. G. Barry, M. Piper, C. Lindwall, R. Moldrich, S. Mason, E. Little, A. Sarkar, S. Tole, R. M. Gronostajski, L. J. Richards, Specific glial populations regulate hippocampal morphogenesis. *J. Neurosci.* **28**, 12328–12340 (2008).
31. Y. H. Heng, R. C. McLeay, T. J. Harvey, A. G. Smith, G. Barry, K. Cato, C. Plachez, E. Little, S. Mason, C. Dixon, R. M. Gronostajski, T. L. Bailey, L. J. Richards, M. Piper, NFIX regulates neural progenitor cell differentiation during hippocampal morphogenesis. *Cereb. Cortex* **24**, 261–279 (2014).
32. J. Dai, K. K. Bercury, J. T. Ahrendsen, W. B. Macklin, Olig1 function is required for oligodendrocyte differentiation in the mouse brain. *J. Neurosci.* **35**, 4386–4402 (2015).
33. Q. R. Lu, T. Sun, Z. Zhu, N. Ma, M. Garcia, C. D. Stiles, D. H. Rowitch, Common developmental requirement for Olig function indicates a motor neuron/oligodendrocyte connection. *Cell* **109**, 75–86 (2002).
34. M. Götz, W. B. Huttner, The cell biology of neurogenesis. *Nat. Rev. Mol. Cell Biol.* **6**, 777–788 (2005).
35. M. Bergsland, D. Ramskold, C. Zaouter, S. Klum, R. Sandberg, J. Muhr, Sequentially acting Sox transcription factors in neural lineage development. *Genes Dev.* **25**, 2453–2464 (2011).
36. S. Klum, C. Zaouter, Z. Alekseenko, A. K. Bjorklund, D. W. Hagey, J. Ericson, J. Muhr, M. Bergsland, Sequentially acting SOX proteins orchestrate astrocyte- and oligodendrocyte-specific gene expression. *EMBO Rep.* **19**, e46635 (2018).
37. The ENCODE Project Consortium, An integrated encyclopedia of DNA elements in the human genome. *Nature* **489**, 57–74 (2012).
38. A. Visel, S. Minovitsky, I. Dubchak, L. A. Pennacchio, VISTA enhancer browser--a database of tissue-specific human enhancers. *Nucleic Acids Res.* **35**, D88–D92 (2007).
39. J. E. Phillips-Cremins, M. E. Sauria, A. Sanyal, T. I. Gerasimova, B. R. Lajoie, J. S. Bell, C. T. Ong, T. A. Hookway, C. Guo, Y. Sun, M. J. Bland, W. Wagstaff, S. Dalton, T. C. McDevitt, R. Sen, J. Dekker, J. Taylor, V. G. Corces, Architectural protein subclasses shape 3D organization of genomes during lineage commitment. *Cell* **153**, 1281–1295 (2013).
40. J. E. Lee, C. Wang, S. Xu, Y. W. Cho, L. Wang, X. Feng, A. Baldridge, V. Sartorelli, L. Zhuang, W. Peng, K. Ge, H3K4 mono- and di-methyltransferase MLL4 is required for enhancer activation during cell differentiation. *eLife* **2**, e01503 (2013).
41. M. P. Creyghton, A. W. Cheng, G. G. Welstead, T. Kooistra, B. W. Carey, E. J. Steine, J. Hanna, M. A. Lodato, G. M. Frampton, P. A. Sharp, L. A. Boyer, R. A. Young, R. Jaenisch, Histone H3K27ac separates active from poised enhancers and predicts developmental state. *Proc. Natl. Acad. Sci. U.S.A.* **107**, 21931–21936 (2010).
42. J. A. Gorski, T. Talley, M. Qiu, L. Puelles, J. L. Rubenstein, K. R. Jones, Cortical excitatory neurons and glia, but not GABAergic neurons, are produced in the Emx1-expressing lineage. *J. Neurosci.* **22**, 6309–6314 (2002).
43. T. Shu, L. J. Richards, Cortical axon guidance by the glial wedge during the development of the corpus callosum. *J. Neurosci.* **21**, 2749–2758 (2001).
44. T. Li, D. Yang, J. Li, Y. Tang, J. Yang, W. Le, Critical role of Tet3 in neural progenitor cell maintenance and terminal differentiation. *Mol. Neurobiol.* **51**, 142–154 (2015).
45. K. D. Rasmussen, I. Berest, S. Kebetaler, K. Nishimura, L. Simon-Carrasco, G. S. Vassiliou, M. T. Pedersen, J. Christensen, J. B. Zaugg, K. Helin, TET2 binding to enhancers facilitates transcription factor recruitment in hematopoietic cells. *Genome Res.* **29**, 564–575 (2019).
46. L. Rinaldi, D. Datta, J. Serrat, L. Morey, G. Solanas, A. Avgustinova, E. Blanco, J. I. Pons, D. Matallanas, A. Von Kriegsheim, L. Di Croce, S. A. Benitah, Dnmt3a and Dnmt3b associate with enhancers to regulate human epidermal stem cell homeostasis. *Cell Stem Cell* **19**, 491–501 (2016).
47. C. Wang, J. E. Lee, B. Lai, T. S. Macfarlan, S. Xu, L. Zhuang, C. Liu, W. Peng, K. Ge, Enhancer priming by H3K4 methyltransferase MLL4 controls cell fate transition. *Proc. Natl. Acad. Sci. U.S.A.* **113**, 11871–11876 (2016).
48. D. C. Becht, S. A. Mohid, J. E. Lee, M. Zandian, C. Benz, S. Biswas, V. K. Sinha, Y. Ivarsson, K. Ge, Y. Zhang, T. G. Kutateladze, MLL4 binds TET3. *Structure* **32**, 706–714.e3 (2024).
49. E. S. Akdemir, A. Y. Huang, B. Deneen, Astrocytogenesis: Where, when, and how. *F1000Res* **9**, F1000 (2020).
50. G. Fan, K. Martinowich, M. H. Chin, F. He, S. D. Fouse, L. Hutnick, D. Hattori, W. Ge, Y. Shen, H. Wu, J. ten Hoeve, K. Shuai, Y. E. Sun, DNA methylation controls the timing of astrogliogenesis through regulation of JAK-STAT signaling. *Development* **132**, 3345–3356 (2005).
51. F. He, H. Wu, L. Zhou, Q. Lin, Y. Cheng, Y. E. Sun, Tet2-mediated epigenetic drive for astrocyte differentiation from embryonic neural stem cells. *Cell Death Discov.* **6**, 30 (2020).
52. G. Steele-Perkins, C. Plachez, K. G. Butz, G. Yang, C. J. Bachurski, S. L. Kinsman, E. D. Litwack, L. J. Richards, R. M. Gronostajski, The transcription factor gene Nfib Is essential for both lung maturation and brain development. *Mol. Cell. Biol.* **25**, 685–698 (2005).
53. T. Sanosaka, T. Imamura, N. Hamazaki, M. Chai, K. Igarashi, M. Ideta-Otsuka, F. Miura, T. Ito, N. Fujii, K. Ikeo, K. Nakashima, DNA methylome analysis identifies transcription factor-based epigenomic signatures of multilineage competence in neural stem/progenitor cells. *Cell Rep.* **20**, 2992–3003 (2017).
54. F. Bandeira, R. Lent, S. Herculano-Houzel, Changing numbers of neuronal and non-neuronal cells underlie postnatal brain growth in the rat. *Proc. Natl. Acad. Sci. U.S.A.* **106**, 14108–14113 (2009).
55. M. Zhang, J. Wang, K. Zhang, G. Lu, Y. Liu, K. Ren, W. Wang, D. Xin, L. Xu, H. Mao, J. Xing, X. Gao, W. Jin, K. Berry, K. Mikoshiba, S. Wu, Q. R. Lu, X. Zhao, Ten-eleven translocation 1 mediated-DNA hydroxymethylation is required for myelination and remyelination in the mouse brain. *Nat. Commun.* **12**, 5091 (2021).
56. W. Choi, M. S. Choe, S. M. Kim, S. J. Kim, J. Lee, Y. Lee, S. M. Lee, S. H. Dho, M. Y. Lee, L. K. Kim, RFX4 is an intrinsic factor for neuronal differentiation through induction of proneural genes POU3F2 and NEUROD1. *Cell. Mol. Life Sci.* **81**, 99 (2024).
57. M. H. Dominguez, A. E. Ayoub, P. Rakic, POU-III transcription factors (Brn1, Brn2, and Oct6) influence neurogenesis, molecular identity, and migratory destination of upper-layer cells of the cerebral cortex. *Cereb. Cortex* **23**, 2632–2643 (2013).
58. E. Stoyanova, M. Riad, A. Rao, N. Heintz, 5-Hydroxymethylcytosine-mediated active demethylation is required for mammalian neuronal differentiation and function. *eLife* **10**, e66973 (2021).
59. L. Ma, Q. Tang, X. Gao, J. Lee, R. Lei, M. Suzuki, D. Zheng, K. Ito, P. S. Frenette, M. M. Dawlaty, Tet-mediated DNA demethylation regulates specification of hematopoietic stem and progenitor cells during mammalian embryogenesis. *Sci. Adv.* **8**, eabm3470 (2022).
60. J. C. Flores, S. Sidoli, M. M. Dawlaty, Tet2 regulates Sin3a recruitment at active enhancers in embryonic stem cells. *iScience* **26**, 107170 (2023).
61. H. Wang, H. Yang, C. S. Shivalila, M. M. Dawlaty, A. W. Cheng, F. Zhang, R. Jaenisch, One-step generation of mice carrying mutations in multiple genes by CRISPR/Cas-mediated genome engineering. *Cell* **153**, 910–918 (2013).
62. H. C. Ketchum, M. Suzuki, M. M. Dawlaty, Catalytic-dependent and -independent roles of TET3 in the regulation of specific genetic programs during neuroectoderm specification. *Commun. Biol.* **7**, 415 (2024).
63. M. Gouti, A. Tsakiridis, F. J. Wymeersch, Y. Huang, J. Kleinjung, V. Wilson, J. Briscoe, In vitro generation of neuromesodermal progenitors reveals distinct roles for wnt signalling in the specification of spinal cord and paraxial mesoderm identity. *PLOS Biol.* **12**, e1001937 (2014).
64. G. Belenguer, A. Domingo-Muelas, S. R. Ferron, J. M. Morante-Redolat, I. Farinas, Isolation, culture and analysis of adult subependymal neural stem cells. *Differentiation* **91**, 28–41 (2016).
65. Y. Qin, C. Zhou, N. Wang, H. Yang, W. Q. Gao, Conversion of adipose tissue-derived mesenchymal stem cells to neural stem cell-like cells by a single transcription factor, sox2. *Cell. Reprogram.* **17**, 221–226 (2015).
66. E. Lujan, S. Chanda, H. Ahlenius, T. C. Sudhof, M. Wernig, Direct conversion of mouse fibroblasts to self-renewing, tripotent neural precursor cells. *Proc. Natl. Acad. Sci. U.S.A.* **109**, 2527–2532 (2012).
67. C. Zhang, Z. Ji, M. Wang, W. Zhang, R. Yang, H. An, R. Yang, D. van Abel, M. van Dijk, X. Yang, G. Ou, H. H. Zhu, W. Q. Gao, Stox1 as a novel transcriptional suppressor of Math1 during cerebellar granule neurogenesis and medulloblastoma formation. *Cell Death Differ.* **23**, 2042–2053 (2016).
68. Y. Yu, Y. Chen, B. Kim, H. Wang, C. Zhao, X. He, L. Liu, W. Liu, L. M. Wu, M. Mao, J. R. Chan, J. Wu, Q. R. Lu, Olig2 targets chromatin remodelers to enhancers to initiate oligodendrocyte differentiation. *Cell* **152**, 248–261 (2013).

69. A. Dobin, C. A. Davis, F. Schlesinger, J. Drenkow, C. Zaleski, S. Jha, P. Batut, M. Chaisson, T. R. Gingeras, STAR: Ultrafast universal RNA-seq aligner. *Bioinformatics* **29**, 15–21 (2013).
70. M. I. Love, W. Huber, S. Anders, Moderated estimation of fold change and dispersion for RNA-seq data with DESeq2. *Genome Biol.* **15**, 550 (2014).
71. B. T. Sherman, M. Hao, J. Qiu, X. Jiao, M. W. Baseler, H. C. Lane, T. Imamichi, W. Chang, DAVID: A web server for functional enrichment analysis and functional annotation of gene lists (2021 update). *Nucleic Acids Res.* **50**, W216–W221 (2022).
72. Y. Chen, Y. Chen, C. Shi, Z. Huang, Y. Zhang, S. Li, Y. Li, J. Ye, C. Yu, Z. Li, X. Zhang, J. Wang, H. Yang, L. Fang, Q. Chen, SOAPnuke: A MapReduce acceleration-supported software for integrated quality control and preprocessing of high-throughput sequencing data. *Gigascience* **7**, 1–6 (2018).
73. F. Krueger, S. R. Andrews, Bismark: A flexible aligner and methylation caller for Bisulfite-Seq applications. *Bioinformatics* **27**, 1571–1572 (2011).
74. P. Danecek, J. K. Bonfield, J. Liddle, J. Marshall, V. Ohan, M. O. Pollard, A. Whitwham, T. Keane, S. A. McCarthy, R. M. Davies, H. Li, Twelve years of SAMtools and BCFtools. *Gigascience* **10**, giab008 (2021).
75. Q. Song, B. Decato, E. E. Hong, M. Zhou, F. Fang, J. Qu, T. Garvin, M. Kessler, J. Zhou, A. D. Smith, A reference methylome database and analysis pipeline to facilitate integrative and comparative epigenomics. *PLOS ONE* **8**, e81148 (2013).
76. A. R. Quinlan, I. M. Hall, BEDTools: A flexible suite of utilities for comparing genomic features. *Bioinformatics* **26**, 841–842 (2010).
77. G. Yu, L. G. Wang, Q. Y. He, ChIPseeker: An R/Bioconductor package for ChIP peak annotation, comparison and visualization. *Bioinformatics* **31**, 2382–2383 (2015).
78. S. Heinz, C. Benner, N. Spann, E. Bertolino, Y. C. Lin, P. Laslo, J. X. Cheng, C. Murre, H. Singh, C. K. Glass, Simple combinations of lineage-determining transcription factors prime cis-regulatory elements required for macrophage and B cell identities. *Mol. Cell* **38**, 576–589 (2010).
79. K. S. Pollard, M. J. Hubisz, K. R. Rosenbloom, A. Siepel, Detection of nonneutral substitution rates on mammalian phylogenies. *Genome Res.* **20**, 110–121 (2010).
80. W. J. Kent, A. S. Zweig, G. Barber, A. S. Hinrichs, D. Karolchik, BigWig and BigBed: Enabling browsing of large distributed datasets. *Bioinformatics* **26**, 2204–2207 (2010).
81. F. Ramirez, D. P. Ryan, B. Gruning, V. Bhardwaj, F. Kilpert, A. S. Richter, S. Heyne, F. Dundar, T. Manke, deepTools2: A next generation web server for deep-sequencing data analysis. *Nucleic Acids Res.* **44**, W160–W165 (2016).
82. L. Lopez-Delisle, L. Rabbani, J. Wolff, V. Bhardwaj, R. Backofen, B. Gruning, F. Ramirez, T. Manke, pyGenomeTracks: Reproducible plots for multivariate genomic datasets. *Bioinformatics* **37**, 422–423 (2021).
83. H. S. Kaya-Okur, S. J. Wu, C. A. Codomo, E. S. Pledger, T. D. Bryson, J. G. Henikoff, K. Ahmad, S. Henikoff, CUT&Tag for efficient epigenomic profiling of small samples and single cells. *Nat. Commun.* **10**, 1930 (2019).
84. B. Langmead, S. L. Salzberg, Fast gapped-read alignment with Bowtie 2. *Nat. Methods* **9**, 357–359 (2012).
85. M. P. Meers, D. Tenenbaum, S. Henikoff, Peak calling by sparse enrichment analysis for CUT&RUN chromatin profiling. *Epigenetics Chromatin* **12**, 42 (2019).
86. C. S. Ross-Innes, R. Stark, A. E. Teschendorff, K. A. Holmes, H. R. Ali, M. J. Dunning, G. D. Brown, O. Gojis, I. O. Ellis, A. R. Green, S. Ali, S. F. Chin, C. Palmieri, C. Caldas, J. S. Carroll, Differential oestrogen receptor binding is associated with clinical outcome in breast cancer. *Nature* **481**, 389–393 (2012).
87. S. Wingett, P. Ewels, M. Furlan-Magaril, T. Nagano, S. Schoenfelder, P. Fraser, S. Andrews, HiCUP: Pipeline for mapping and processing Hi-C data. *F1000Res* **4**, 1310 (2015).
88. J. Cairns, P. Freire-Pritchett, S. W. Wingett, C. Varnai, A. Dimond, V. Plagnol, D. Zerbino, S. Schoenfelder, B. M. Javierre, C. Osborne, P. Fraser, M. Spivakov, CHiCAGO: Robust detection of DNA looping interactions in capture Hi-C data. *Genome Biol.* **17**, 127 (2016).
89. K. Ito, J. Lee, S. Chrysanthou, Y. Zhao, K. Josephs, H. Sato, J. Teruya-Feldstein, D. Zheng, M. M. Dawlaty, K. Ito, Non-catalytic roles of Tet2 are essential to regulate hematopoietic stem and progenitor cell homeostasis. *Cell Rep.* **28**, 2480–2490.e4 (2019).

Acknowledgments: We thank the Einstein Epigenomics Facility for help with next-generation sequencing, the Einstein Transgenic Facility for help generating *Emx1*$^{Cre/Cre}$;*Tet3*$^{+/-}$ mice, and the Skoultchi laboratory at Einstein for providing reagents for CUT&Tag. We are grateful to J. T. Gonçalves, K. Dobrenis, and K. Jackson for advice on brain fixation, cryosectioning, and staining. We are grateful to J. Hébert and all Dawlaty laboratory members for critical reading of the manuscript. **Funding:** This work was in part supported by funds to M.M.D. from NIH R01GM122839 and the Einstein Rose F Kennedy Intellectual and Developmental Disabilities Research Center (IDDRC) pilot grant. M.M.D. was also supported by NIH R01HL148852, Hirschl Trust Funds, and funds from Albert Einstein College of Medicine Stem Cell Institute and Genetics Department. I.C.M. was supported by NIH predoctoral fellowship F30HD107921 and Medical Scientist Training Program training grant T32GM149364. L.M. was, in part, supported by the Einstein Training Program in Stem Cell Research from the Empire State Stem Cell Fund NYSDOH Contract C30292GG. **Authors contributions:** Conceptualization: I.C.M., L.M., C.-Y.H., and M.M.D. Investigation: I.C.M., L.M., C.-Y.H., and H.B. Methodology: I.C.M., L.M., C.-Y.H., and M.M.D. Resources: I.C.M., L.M., C.-Y.H., M.S., and M.M.D. Software: C.-Y.H. and M.S. Data curation: I.C.M. and C.-Y.H. Validation: I.C.M. and C.-Y.H. Formal analysis: I.C.M. and C.-Y.H. Visualization: I.C.M., L.M., and C.-Y.H. Writing—original draft: I.C.M., C.-Y.H., and M.M.D. Writing—review and editing: I.C.M., L.M., C.-Y.H., M.S., and M.M.D. Project administration: I.C.M., C.-Y.H., and M.M.D. Funding acquisition: I.C.M. and M.M.D. Supervision: I.C.M., C.-Y.H., and M.M.D. **Competing interests:** The authors declare that they have no competing interests. **Data and materials availability:** All data needed to evaluate the conclusions in the paper are present in the paper and/or the Supplementary Materials. The RNA-seq, CUT&Tag, WGBS, and promoter capture HiC data have been deposited in the Gene Expression Omnibus (GEO) database accession number (GSE248933) and are publicly available.

Submitted 7 February 2024
Accepted 24 July 2024
Published 28 August 2024
10.1126/sciadv.ado5424